

DASH: A MATLAB Toolbox for Paleoclimate Data Assimilation

Jonathan King^{1,2}, Jessica Tierney¹, Matthew Osman^{1,3}, Emily J. Judd⁴, and Kevin J. Anchukaitis^{1,2,5}

¹Department of Geosciences, University of Arizona, Tucson, Arizona, USA

²Laboratory of Tree Ring Research, University of Arizona, Tucson, Arizona, USA

³Department of Geography, University of Cambridge, Cambridge, UK

⁴Department of Paleobiology, Smithsonian National Museum of Natural History, Washington, DC, USA

⁵School of Geography, Development, and Environment, University of Arizona, Tucson, Arizona, USA

Correspondence: Jonathan King (jonking93@email.arizona.edu)

Abstract. Paleoclimate data assimilation (DA) is a **novel** tool for reconstructing past climates that directly integrates proxy records with climate model output. Despite the potential for DA to expand the scope of quantitative paleoclimatology, these methods remain difficult to implement in practice due to the multi-faceted requirements and data handling necessary for DA reconstructions, the diversity of DA methods, and the need for computationally efficient algorithms. Here, we present DASH, a

5 MATLAB toolbox designed to facilitate paleoclimate DA analyses. DASH provides command line and scripting tools that implement common tasks in DA workflows. The toolbox is highly modular and is not built around any specific analysis, and thus DASH supports paleoclimate DA for a wide variety of time periods, spatial regions, proxy networks, and algorithms. DASH includes tools for integrating and cataloguing data stored in disparate formats, building state vector ensembles, and running proxy (system) forward models. The toolbox also provides optimized algorithms for implementing ensemble Kalman filters, 10 particle filters, and optimal sensor analyses with variable and modular parameters. This paper reviews the key components of the DASH toolbox and presents examples illustrating DASH's use for paleoclimate DA applications.

1 Introduction

Past climates provide insight into the drivers, variability, and evolution of the Earth's climate system, and are invaluable for providing insight on the consequences of current and future anthropogenic climate change (Alley, 2003; Hargreaves et al.,

15 2007; Rice et al., 2009; Schmidt, 2010; Snyder, 2010; Ault et al., 2014; Coats et al., 2020; Tierney et al., 2020a). Paleoclimate studies can help constrain important climate system properties including Equilibrium Climate Sensitivity (Hegerl et al., 2006; Rohling et al., 2012; Hansen et al., 2013; Kutzbach et al., 2013; Rohling et al., 2018; Sherwood et al., 2020; Tierney et al., 2020b; Zhu et al., 2020b), quantify internal and forced variability across a range of timescales and climate system metrics (Cane et al., 2006; Cook et al., 2011; Goosse et al., 2012a; Ault et al., 2013; Fernández-Donado et al., 2013; Anchukaitis et al., 2019; Neukom et al., 2019; Fang et al., 2021), and can serve as analogues for future warm climate states projected to occur due to anthropogenic warming (Overpeck et al., 2006; Burke et al., 2018; Tierney et al., 2020a, 2022). Reconstructions of past climates also provide out-of-sample targets used to assess the skill of climate models, which in turn helps constrain future

projections and enables superior climate change adaptation strategies (Crowley, 1991; Hargreaves and Annan, 2009; Schmidt et al., 2013; Zhu et al., 2021a, b; Gulev et al., 2021).

25 Beyond the limited period of instrumental climate observations, researchers have primarily relied on two methods for studying past climates: proxy reconstructions and climate model hindcasts. In a proxy reconstruction, paleoclimatologists use climate proxy records, such as tree rings, ice cores, speleothems, corals, and lake and marine sediments, to make statistical estimates of past climates. These reconstructions rely on a combination of empirical and process-based understanding to link proxy records to features and characteristics of the Earth's climate system. A major advantage of using proxy data to reconstruct
30 past climates is that they produce estimates of temperature, precipitation, or other climate variables that are consistent with the actual trajectory of the Earth's climate system. These reconstructions can also provide independent validation of climate model performance. However, many factors can hinder the inference of past climates from proxy data. These factors include the sparse distribution of proxy records through space and time, time-uncertainty due to limits on the precision of geochronology, and the influence of multivariate or non-climatic factors on proxy records. Furthermore, the physical processes that archive
35 climate signals in proxy records can be complex and are often not completely understood, which complicates the extraction of climate signals from proxy data using linear, univariate, and empirical statistical approaches. Proxy records are sensitive to the local climates in which they form, but many reconstructions target large-scale climate features or ocean-atmosphere modes not directly sensed by the available proxy data. Some reconstructions derive relationships between proxy records and target variables using calibrations with the instrumental era; however, due to the effects of anthropogenic climate forcings, modern climate is not in equilibrium and ~~continues to respond to increasing anthropogenic climate forcings~~does not necessarily resemble the climate of the past. Therefore, modern teleconnections and climate-system spatial covariance patterns may differ from long-term and unforced patterns. Finally, many proxy reconstruction methods assume that teleconnections between local- and large-scale climate variables are stationary over reconstruction periods, an assumption that may not hold in reality.

40 Climate model hindcasts leverage general circulation models to simulate past climate states using estimates of past boundary conditions, such as the Earth's orbital parameters, atmospheric greenhouse gas concentrations, volcanic eruptions, continental configurations, and land cover. By contrast with proxy reconstructions, climate model hindcasts simulate data for target climate variables at all spatial points and time steps within the model domain. Furthermore, these simulated climate variables evolve according to fundamental physical governing equations and parameterizations, rather than the statistical associations and assumptions typically used for proxy reconstructions. Consequently, paleoclimate simulations can provide insight into the physical mechanisms behind reconstructed climate phenomena. However, no model fully captures the real Earth system, and determining appropriate boundary conditions becomes increasingly difficult going back through geologic time, so all paleoclimate hindcasts necessarily contain errors in their representation of past climates. Additionally, many model variables are dominated by internal variability, sensitivity to initial conditions, and/or chaotic behavior over a range of time periods (Deser et al., 2012). Thus, no individual simulation will capture the true or specific trajectory of the Earth's past climate; instead, each
45 simulation represents a single possible trajectory in a distribution of physically-plausible past climate states (e.g. Kay et al., 2015). Finally, climate models require external validation to evaluate their fidelity and accuracy in reproducing past climate states.

Recently, data assimilation (DA) methods have emerged as ~~a novel~~an additional approach to the problems and challenges of paleoclimate reconstruction (e.g. ~~Bhend et al., 2012; Goosse et al., 2012b; Mairesse et al., 2013; Hakim et al., 2016; Steiger et al., 2017, 2019~~
60 e.g. LeGrand and Wunsch, 1995; Mairesse et al., 2013; Gebbie, 2014; Steiger et al., 2017; Kurahashi-Nakamura et al., 2017; Amrhein et al., 2019). Unlike the two independent approaches described above, DA methods integrate proxy data directly with climate model output and thereby leverage the strengths of both information sources. Because they utilize climate model simulations, DA methods can provide full-field global reconstructions (e.g. Evans et al., 2001) for nearly any simulated climate parameter, since the relationships between variables are linked through the physically based governing equations of the model. Simultaneously, DA
65 reconstructions are constrained by proxy records and thus reflect the true trajectory of the Earth's past climate. DA methods use forward models to describe how climate signals are sensed by and recorded in proxy archives, and thus can incorporate proxy system physical processes that are multivariate or nonlinear. Furthermore, the use of proxy forward models allows DA methods to relax calibration requirements when attempting to reconstruct large-scale climate modes or fields, such that proxy data can be calibrated to local climate variables rather than directly to large-scale teleconnections. DA methods can also relax assumptions of teleconnection stationarity, as the effects of changing climate boundary conditions can be reflected in the evolution of climate model output and its covariance.
70

~~Despite the potential strengths of paleoclimate DA, However, DA is not a perfect method, and it is important to also acknowledge its limitations. For example, although DA methods can reconstruct nearly any climate parameter, there is no guarantee that the reconstruction will be skillful. Additionally, the interaction of climate model, proxy data, and forward model~~
75 uncertainties can severely reduce reconstruction skill in some cases. Finally, certain DA techniques can create artifacts in the temporal variability of reconstructions or result in physically implausible reconstructions. We refer readers to Section 5 for a more detailed discussion of these concerns, as well as potential solutions.

An additional issue for paleoclimate DA is that these reconstructions are often difficult to implement in practice. DA analyses require numerous discrete tasks, including preparing and integrating the output from climate model simulations, proxy records, 80 and possibly instrumental data, all of which may use different data formats, units, and metadata. The number of potential reconstruction targets and proxy variables is immense, and the choice of algorithm parameters will affect the implementation of any particular DA reconstruction (compare Tardif et al., 2019; Tierney et al., 2020b; King et al., 2021; Osman et al., 2021; King et al., 2023). Consequently, it can be difficult to adapt codes implementing an existing reconstruction to alternative applications. Paleoclimate DA also encompasses a diverse array of algorithms and algorithm variants (compare Goosse et al., 85 2006; Dubinkina and Goosse, 2013; Steiger et al., 2014; Matsikaris et al., 2015; Comboul et al., 2015; Dee et al., 2016; Acevedo et al., 2017; Liu et al., 2017; Perkins and Hakim, 2017; Franke et al., 2020), further increasing the complexity of implementing DA codes. Finally, DA methods are often computationally intensive and require both optimized algorithms and efficient use of computer memory, and these considerations can dissuade potential users lacking experience or access to high-performance computing.
90

Although DA software does exist, thus far these packages are not suitable for generalized paleoclimate applications with a diverse range of time scales, climate model requirements, and proxy data types. Packages designed to implement general DA methods typically lack support for fundamental components of paleoclimate DA, such as the use of proxy forward models.

By contrast, DA packages designed for paleoclimate applications, such as the [LMR \(Hakim et al., 2016; Tardif et al., 2019\)](#) or [PHYDA \(Steiger et al., 2018\)](#) [Last Millennium Reanalysis \(LMR; Hakim et al., 2016; Tardif et al., 2019\)](#) or the [Paleo Hydrodynamics Data Assimilation codebase \(PHYDA; Steiger et al., 2018\)](#), have been built to implement specific analyses, use particular proxy data, or incorporate specified climate model inputs. Adapting these products for generalized paleoclimate applications requires modifying the source code, which may be difficult or time-intensive and thus presents a barrier to their use.

A second difficulty for paleoclimatologists seeking to implement DA is that the methods are comparatively complex relative to existing reconstruction methods. Describing experimental DA setups in sufficient detail to allow reproducibility requires considerable length, and published methods may focus of the broad scope of the mathematics while neglecting the details of key implementation steps in favor of brevity. Additionally, there are still relatively few paleoclimate applications in the mathematical DA literature, so DA descriptions may use a variety of mathematical notations. Finally, the diversity of algorithm variants potentially hinders transparency and accessibility, as studies using similarly named algorithms may implement different methods in practice (compare Tardif et al., 2019; Franke et al., 2020; Tierney et al., 2020b; King et al., 2023). Ultimately, there are limited frameworks for discussing DA within the paleoclimate literature, and the field as a whole would benefit from more transparent implementations that do not require additional specialized training.

In this paper, we present DASH, a MATLAB toolbox supporting paleoclimate data assimilation. The toolbox is designed for general paleoclimate DA and is not built around ~~or for~~ any particular analysis, time period, proxy type, or climate model. Consequently, the toolbox is highly modular and allows flexible implementation of diverse DA analyses. DASH provides command line / scripting utilities designed to implement common tasks for paleoclimate DA workflows, with a goal of improving access to DA methods for users with diverse scientific backgrounds. DASH includes support for organizing climate data, building state vector ensembles, running proxy forward models, and implementing standard DA algorithms. All algorithms are optimized for both speed and efficient memory use. Our goal is for DASH to improve clarity and transparency in DA analyses and provide a framework for paleoclimate DA discussions. Consequently, DASH commands are designed to provide a description of their routines, thereby promoting the creation of human-readable DA scripts.

The remainder of this paper is organized as follows. In Section 2, we present a brief overview of paleoclimate DA, with the aim of introducing common tasks, data, and algorithms for paleoclimate DA workflows. In Section 3, we describe the DASH toolbox specifically. We detail its general characteristics and layout and highlight its major components. In Section 4, we provide two examples that use DASH to implement paleoclimate data assimilation. These examples use different temporal periods, spatial regions, proxy networks, and algorithms in order to demonstrate the flexibility of the DASH toolbox. ~~Finally, in~~ [In](#) Section 5 we provide a set of best practices and caveats ~~, discuss for using paleoclimate DA. Section 6 discusses~~ the DASH toolbox in the broader context of paleoclimate DA ~~, and outline and outlines~~ potential and anticipated future developments to the code. [Finally, Section 7 provides concluding remarks.](#)

2 Overview of Paleoclimate DA

125 This section provides a brief overview of paleoclimate data assimilation, with the goal of introducing DA to paleoclimate
researchers who may not be familiar with the broader mathematical DA literature. In particular, we aim to (1) ~~Provide~~ provide
accessible insight into the DA “black-box”, (2) improve the transparency of common DA algorithms, (3) establish a vocabulary
for DA workflows, and (4) provide context for the DASH software package. We focus on illustrating the tasks and quantitative
routines most frequently used in paleoclimate DA workflows, rather than providing complete mathematical descriptions (which
130 can be found elsewhere, e.g. Evensen (1994); Van Leeuwen (2009)). Here, we focus specifically on the ensemble Kalman
filter and ensemble particle filter methods. We also describe an optimal sensor algorithm based on an ensemble Kalman filter
framework. Additional and more complete descriptions of DA algorithms are available in Evensen (1994); Anderson and
Anderson (1999); Whitaker and Hamill (2002); Goosse et al. (2006, 2012b); Dubinkina and Goosse (2013); Steiger et al.
(2014); Comboul et al. (2015); Hakim et al. (2016); Tardif et al. (2019); Franke et al. (2020); Tierney et al. (2020b); King et al.
135 (2021); Osman et al. (2021).

2.1 Conceptual framework

In the broadest terms, DA methods combine output from climate model simulations (X_p) with ~~observations or~~ proxy records
(Y) to reconstruct a set of climate variables (X_a).

$$X_a = f(X_p, Y) \quad (1)$$

140 The reconstructed climate variables X_a , also known as the analysis, are calculated by updating climate variables from the
climate models X_p to more closely match the proxy records Y. The Kalman filter and particle filter methods discussed in
this paper can also be formulated as Bayesian filters (Chen et al., 2003; Wikle and Berliner, 2007) wherein new information
(Y) is used to update estimates of state parameters (X). Hence, we will often refer to X_p and X_a as the *prior* and *posterior*,
respectively.

145 ~~When discussing DA, it is important to distinguish between online and offline modes. In an online regime, the assimilation
updates are used to inform the evolution of the climate model simulations. Essentially, the updated ensemble for a given time
step informs the starting states of the climate model simulations in the next time step. Equivalently, X_p becomes a function
of the proxy records from previous time steps. By contrast, in offline DA all climate model output is generated in advance,
and so the assimilation updates do not inform the evolution of the climate model simulations (Oke et al., 2002; Evensen, 2003)~~
150 ~~. Offline methods incur a significantly lower computational cost than online methods, but the priors of the reconstructed time
steps are not constrained by the proxy records (Oke et al., 2002; Evensen, 2003; Matsikaris et al., 2015; Acevedo et al., 2017)~~
~~. As such, researchers must consider both computational feasibility and the propagation of proxy information when choosing
between the online and offline modes.~~

In general, climate model output is organized into *state vectors*, which consist of multi-dimensional spatiotemporal climate
155 model output reshaped into a vector of data values (Figure 1, ~~upper left~~a). There is no strict definition for the contents of a

state vector, but they typically include data for one or more climate variables ~~at a set of~~, possibly at multiple spatial points. ~~A state vector~~ This data may be time-averaged or might also contain a trajectory of successive points in time; for example, individual months of the year or a number of successive years following an event of interest. Essentially, a state vector serves as a possible description of the climate system for some period of time. In this paper, we focus on *ensemble* DA methods, 160 which rely on state vector ensembles. A *state vector ensemble* is a collection of multiple state vectors organized in a matrix (Figure 1, ~~upper right~~b), and a given ensemble provides an empirical distribution of possible climate states. For paleoclimate applications, ensemble members are often selected from different points in time, different members of an initial condition, perturbed physics, or multi-model ensemble, or a combination of these options. In a typical DA algorithm, the state vectors in an ensemble are compared to a set of proxy record values for a given time ~~step or time~~ slice. Essentially, the method compares 165 the potential descriptions of the climate system taken from the climate model to the proxy values from the real past climate record. The similarity of each state vector to the set of proxy records is then used to inform the final reconstruction.

In order to compare state vectors with a set of proxy record values, DA methods must transfer state vectors and proxy records into a common unit space. This is accomplished by applying proxy forward models (Evans et al., 2013) to relevant climate variables stored in each state vector (Figure 1, ~~bottom left~~c). For a given state vector, a forward model is run for each proxy 170 record in \hat{Y} , using the relevant climate variables in the state vector as inputs. This produces a set of values in the same units as the proxy records and therefore allows direct comparison of the state vector and observed proxy values. In general, DA methods will run a forward model to estimate each proxy record for each state vector in an ensemble; the collective outputs are referred to as *proxy estimates* (\hat{Y}) and allow comparison of the states in the ensemble with a set of proxy records. The proxy estimates are often expressed using the notation:

$$175 \quad \hat{Y} = H X_p \quad (2)$$

where H is an operator representing the proxy forward models applied to the prior ensemble X_p . The difference between the proxy observations and proxy estimates is known as the *innovation* (Figure 1, ~~bottom right~~d):

$$\text{innovation} = Y - \hat{Y} \quad (3)$$

and describes the discrepancies between the actual proxy records and the climate states in the ensemble. The innovation is then 180 used to constrain or update the prior ensemble (X_p) to more closely resemble the observed proxy records.

In addition to proxy innovations, the DA methods detailed here also consider proxy uncertainties (R) when comparing state vectors to the proxy records, such that:

$$X_a = f(X_p, Y, R) \quad (4)$$

In this way, proxy records with high uncertainties are given less weight in the reconstruction. In classical assimilation frame- 185 works, R is often derived from the uncertainty inherent in measuring an observed quantity. For example, R might reflect the uncertainty of width measurements in a tree-ring chronology. However, in nearly all paleoclimate applications, measurement uncertainties are small compared to (1) the uncertainties inherent in proxy forward models, ~~and~~(2) uncertainties resulting from

non-climate signals (i.e. noise) archived in the proxy records, and (3) representativeness errors caused by comparing proxy values at points in space or time to model values representing larger spatial or temporal averages. Thus, in paleoclimate DA 190 the proxy uncertainties R must account for proxy noise and forward model errors, and representativeness errors, as well as the covariance between different proxy uncertainties. Most generally, R is the proxy error-covariance matrix. This matrix is diagonal when proxy errors are assumed uncorrelated; otherwise, R is a full covariance matrix.

2.2 Update equations and algorithms

There are several different algorithms that can be used to pass the new information produced by the innovation into the climate 195 models combine the information contained in the prior and the innovation. One of the most commonly used methods in paleoclimate applications is the Kalman Filter-filter (Kalman, 1960; Andrews, 1968; Evensen, 1994), and its update equation is given by:

$$X_a = X_p + K(Y - \hat{Y}) \quad (5)$$

Equation 5 shows that the innovation is weighted by the Kalman Gain matrix (K) in order to compute an update for each 200 state vector in the prior ensemble (X_p). The Kalman Gain weighting considers multiple factors, including (1) the covariance of the proxy estimates (\hat{Y}) with target climate variables (X_p), (2) the covariance between the proxy estimates (\hat{Y}), and (3) the uncertainties in the proxies (R), such that:

$$K = \text{cov}(X, \hat{Y})[\text{cov}(\hat{Y}) + R]^{-1} \quad (6)$$

Applying the updates produces an updated (posterior) ensemble (X_a) with climate states that more closely resemble those 205 recorded by the real proxy records (Y). The ensemble nature of X_a is advantageous because the distribution of climate variables across X_a can help quantify the uncertainty in the reconstruction.

By contrast with Kalman filters, particle filters (Van Leeuwen, 2009) combine the innovation with proxy record uncertainties 210 (R) to compute a weight for each state vector in the ensemble. The reconstruction is then calculated as a weighted mean of the state vectors in the ensemble. Classical particle filters compute these weights using a Bayesian scheme, such that each state vector i is first assigned an importance weight:

$$s_i = \exp\left[-\frac{1}{2} (Y - \hat{Y}_i)^T R (Y - \hat{Y}_i)\right] \quad (7)$$

and then importance weights are normalized to give the final state vector weights:

$$w_i = \frac{s_i}{\sum_{j=1}^N s_j} \quad (8)$$

However, classical particle filters can suffer from degeneracy in the high-dimensional systems common to paleoclimate DA. 215 Essentially, a single ensemble member receives a weight of 1, whereas all other ensemble members receive near-zero weights. When this occurs, reconstructed values (X_a) resemble the single state vector most similar to the proxy records, rather than

values across an ensemble. A common correction for degeneracy involves using the mean of the N state vectors with the highest Bayesian weights. Alternatively, the “degenerate particle filter” refers to the case when the single best state vector is used as the reconstruction (e.g. Goosse et al., 2006, 2010). The “analogue method” may also refer to a degenerate particle filter (e.g. Goosse et al., 2006), although the meaning of this term varies throughout the paleoclimate literature.

When discussing Kalman and particle filters, it is important to distinguish between offline and online regimes. In an online regime, the assimilation updates are used to inform the evolution of the climate model simulations. Essentially, the updated ensemble for a given time step informs the starting states of the climate model simulations in the next time step. By contrast, in the offline regime all climate model output is generated in advance, and so the assimilation updates do not inform the evolution of the climate model simulations (Oke et al., 2002; Evensen, 2003). Offline methods incur a significantly lower computational cost than online methods, but the priors of the reconstructed time steps are not constrained by the proxy records (Oke et al., 2002; Evensen, 2003; Matsikaris et al., 2015; Acevedo et al., 2017). As such, researchers must consider both computational feasibility and the propagation of proxy information when choosing between the online and offline modes.

The optimal sensor algorithm described in this paper follows the method presented by Comboul et al. (2015). This method is derived from an ensemble Kalman filter and complements the reconstruction framework by providing additional information about the contribution of proxy data sites to the reconstruction. In paleoclimatepaleoclimatology, optimal sensor analyses have traditionally been used to evaluate the potential of new proxy sites, to prioritize future proxy development, and to assess the proxy network (i.e. the collection of proxy records) necessary to skillfully reconstruct a climate field (e.g. Bradley, 1996; Evans et al., 1998; Comboul et al., 2015). Here, we expand the method to assess the relative influence of individual proxy records on a reconstructed index.

Rather than reconstructing climate variables over time, the algorithm instead tests the ability of ~~a~~each proxy record to reduce the variance of a scalar climate metric J across an ensemble. ~~A~~Given a set of proxy records (\hat{Y}), the k th proxy record's ability to reduce variance is determined using the covariance of its estimates (\hat{Y}_k) with the climate metric (J), combined with the uncertainty of the proxy record (R). For a given proxy record (y), this proxy record's uncertainty (R_k). This equation is given by:

$$\Delta\sigma_k = \underline{\text{cov}(\hat{y}, J)^2[\text{var}(\hat{y}) + R]^{-1}\text{cov}(\hat{Y}_k, J)^2[\text{var}(\hat{Y}_k) + R_k]^{-1}} \quad (9)$$

where $\Delta\sigma_k$ is the variance reduced by the k th proxy record. This quantity is assessed for each proxy, and the proxy that most strongly reduces variance is selected as the optimal sensor, such that:

$$s_{\text{optimal}} = \underline{\text{argmax}_k \Delta\sigma} \quad (10)$$

~~This~~The optimal proxy is used to update the climate metric using an ensemble Kalman ~~Filter~~filter (Equations 5, 6) and then removed from the network. ~~This analysis~~The algorithm then iterates using the remaining sensors until the desired number of sensors are selected. Ultimately, the method both ranks the proxies in a network and also assesses the total variance reduced by a particular proxy network. This method requires proxy estimates (\hat{Y}) to calculate climate metric covariance but does not use proxy record values themselves (Y), as the potential to reduce ensemble variance is independent of actual proxy values.

3 Description of DASH

3.1 General Characteristics

DASH is a MATLAB toolbox designed to help implement paleoclimate data assimilation. The code is designed for use from the command line as well as within scripts and functions. DASH is written in an object-oriented style, which supports the 255 modularity of the code; the toolbox consists of several classes and packages, each implementing a common task for paleoclimate DA. The code is intended for users with basic previous experience with MATLAB; in particular, users will benefit from knowing how to write a basic `for` loop, and how to index into arrays.

A stated goal of the DASH toolbox is to support the transparency of paleoclimate data assimilation analyses, and the object-oriented design supports this aim. DASH methods are accessed via dot-indexing, which improves clarity by placing sub-tasks 260 within the context of a larger piece of the data assimilation process. Additionally, tasks with many parameters or options are organized into objects, which can store settings between commands. Consequently, the parameters used to implement complex algorithms are split across several commands, improving both the clarity and modularity of codes utilizing DASH.

To support command-line workflows, DASH is designed for console display and does not rely on a graphical user interface (GUI). Users can inspect the state of class objects, assimilation analyses, and other DASH components by displaying them 265 in the console. Users can also examine reference guides for DASH components using the `help` command; however, we recommend that users instead use the HTML documentation set, which is detailed below. Further, we are cognizant that users may not be familiar with all aspects of paleoclimate data assimilation, or with all components of the toolbox. DASH therefore implements robust input checking and error handling for all user-facing methods. Error messages are designed to clearly communicate input failures and suggest possible solutions without requiring users to know the inner workings of the DASH 270 codebase.

The DASH toolbox is accompanied by comprehensive documentation written in HTML. This documentation includes (1) a reference guide for every class, package, method, and function, (2) tutorials for nearly all user-facing commands, and (3) How-Tos and FAQs for common tasks and troubleshooting. The entire documentation can be accessed by entering the `dash.doc` command from the MATLAB command line. Alternatively, users can open the reference manual for a particular component 275 by providing the component name as input: `» dash.doc ("component name")`. The documentation is also available on the project's website (<https://jonking93.github.io/DASH>).

To install DASH, users should first download a stable release of the toolbox, which can be found at the project's Github repository (<https://github.com/JonKing93/DASH/releases>), MATLAB FileExchange (<https://www.mathworks.com/matlabcentral/fileexchange/120453-dash>), or in the MATLAB Add-On Explorer. Then, open the downloaded `DASH-<version>.mltbx` 280 file to complete the installation. We encourage users to download one of the project's stable releases, as the source code on the Github repository's main branch may be in active development and is therefore not configured for quick installation.

3.2 DASH Components

DASH consists of several classes and packages, each implementing a particular task commonly required for paleoclimate data assimilation (Figure 2). In brief, the toolbox contains components to (1) organize and catalogue input data, (2) design 285 and build state vector ensembles, (3) estimate proxy records via proxy forward models, and (4) implement common data assimilation algorithms. In the remainder of this section, we examine the characteristics and features of each of these modules. We realize that many aspects of these classes are abstract in concept, and therefore provide step-by-step tutorials in the DASH documentation that illustrate how DASH works in practice. The examples in Section 4 also demonstrate the use of common DASH commands, albeit in a less detailed style than the tutorials.

290 **3.2.1 Organize Climate Data: `gridfile`, `gridMetadata`**

We begin our overview with the `gridfile` class. This module facilitates the combination of datasets stored in different 295 formats and with disparate metadata by creating data catalogues. The data catalogued within a `gridfile` is associated with user-specified metadata, which allows users to manipulate large datasets using preferred and human-readable metadata formats. This class thereby allows users to consolidate datasets split across multiple files, promotes human-readable data manipulation, and unites disparate data formats within an intuitive framework. The class implements `gridfile` objects, and each object implements a catalogue for data stored in various source files. The basis of each catalogue is an abstract N -dimensional grid, whose scope is defined by user-provided dimensional metadata. This allows users to catalogue datasets of 300 varying dimensionality, while simultaneously tagging data elements with unique and user-preferred metadata values. We note that the grid abstraction does not imply that `gridfile` datasets must use a Cartesian spatial grid. Rather, the class supports a wide-variety of spatial layouts, including rectilinear systems, tripolar grids, randomly distributed spatial sites, and datasets without any spatial component at all.

After first defining the scope of a `gridfile`, users can add data source files to the catalogue by associating the data in each file with a portion of the N -dimensional grid. In this way, the data in each source file is placed within the context of the overall dataset. The `gridfile` package supports data source file formats common in paleoclimate DA – including NetCDF, 305 OPeNDAP, MATLAB’s binary MAT files, and delimited-text files – and individual catalogues may contain any mixture of file formats. The contents of each catalogue are saved in a `.grid` file, so data catalogues can persist across multiple coding sessions. We emphasize that these `.grid` files save only a *catalogue* of a dataset, and not the dataset itself. Thus, `.grid` files do not duplicate data, and individual `.grid` files remain small (typically a few kilobytes) even when they refer to datasets 310 spanning many gigabytes of memory. Once a catalogue is complete, users can return data using the `load` command, which provides a common interface for accessing data in the catalogue. Users can also return a subset of the catalogued data by querying the associated metadata. The `gridfile` class also allows users to apply data transformations, such as log transforms or fill values, to a catalogue. Such transformations are only applied to loaded data, which improves computational efficiency and maintains the data sources as read-only files. Finally, the class allows users to perform arithmetic operations like addition and

multiplication across multiple gridfile datasets; these operations are analogous to several commonly used NetCDF operators

315 but are not limited to NetCDF files.

The gridfile class relies on gridMetadata, which implements objects that define the metadata for a dataset. The gridMetadata class plays an auxiliary role within the DASH toolbox, and is mainly used to define the scope of gridfile catalogues and to locate data subsets within a gridfile dataset. We contrast gridMetadata with ensembleMetadata, a second metadata class implemented by DASH. Whereas gridMetadata characterizes values in an N -dimensional dataset, ensembleMetadata instead characterizes N -dimensional datasets after they are reshaped into state vector ensembles. Further details for the ensembleMetadata class are given in Section 3.2.3.

3.2.2 Build state vector ensembles: `stateVector`, `ensemble`

The next key component of DASH is the stateVector class. This component is designed to facilitate flexible design of state vector ensembles while minimizing the amount of data manipulation done by the user. The class implements objects

325 that hold design parameters required to build a state vector ensemble from gridfile catalogues. To design a state vector,

users first initialize a stateVector object and the climate variables that it will contain. Each variable is associated with a gridfile dataset, and multiple variables in the state vector may be derived from the same dataset (e.g., climate variables representing mean annual and mean summer temperatures could be drawn from the same monthly temperature catalogue). We

note that when a user adds a variable to a stateVector object, no data is loaded into memory at that time. Instead, the object

330 initializes a set of design parameters that can later be used to extract data for the variable from its gridfile. To design the

state vector, users next specify options for the dimensions of the variables. As a first step, users should indicate which dataset dimensions are used to select ensemble members. In most paleoclimate DA applications, ensemble members are selected from different time steps and/or different climate model simulations. However, stateVector is highly flexible and also allows

ensembles built along other dimensions; for example, ensembles built from different height levels or from different spatial

335 locations and sites. Users can also specify a subset of elements along an ensemble dimension to use for building ensemble

members. For example, in a dataset with monthly resolution, a user could specify to only select ensemble members from

January time steps. The class also includes many additional methods for designing state vector variables: users can specify that a variable should be drawn from a subset of a gridfile dataset, or that it should be a computed mean, weighted mean, or sum

340 total over ~~some data dimension~~various data dimensions. Users can also select options for processing variables with different

metadata formats, as well as specify that individual ensemble members should contain temporal sequences. For example, a

variable could include data from individual months of the year, useful for seasonal analyses. Alternatively, a variable could

hold values from successive years, which supports superposed-epoch analyses for climate conditions following discrete events

of interest.

Once a design is complete, users can build the state vector ensemble using the build command. This command loads

345 necessary data from the gridfile catalogues and builds a state vector ensemble according to the specified design parameters.

When building a state vector ensemble, the stateVector class will ensure that all variables within a given ensemble member align to the same metadata values. For example, in an ensemble selected from different time steps, the data for the variables

in each ensemble member will all correspond to the same time step. Similarly, in an ensemble selected from different model simulations, the variables in each ensemble member will all be drawn from the same simulation. The class also ensures that 350 ensemble members are constructed from complete data. For example, if a state vector variable includes a temporal mean or sequence, then the build method will never select an ensemble member for which the mean or sequence would extend outside of the bounds of the dataset.

When building an ensemble, users have the option to return the ensemble directly as an array, or to save the ensemble to a file. This ~~later~~latter option is useful, as state vector ensembles may exceed the size of active memory, particularly when state 355 vectors include multiple spatial fields from high-resolution climate models. In the DASH framework, these files are saved with a `.ens` extension, and the toolbox provides the `ensemble` class to facilitate memory-efficient interactions with saved state vector ensembles. We highlight the ability of the `ensemble` class to selectively load requested state vector rows, variables, and ensemble members into memory. These features have particular utility when running (1) proxy forward models, which typically only require a small subset of ensemble data, and (2) data assimilation algorithms, as many reconstructions only 360 target a subset of variables in an ensemble. Users can also call the `evolving` command to implement evolving offline priors (e.g. Osman et al., 2021) without loading data values to memory.

3.2.3 Proxy Forward Models: `PSM`, `ensembleMetadata`

After building a state vector ensemble, a common next task in paleoclimate DA is to design a forward model for each proxy record. These forward models are either used to generate proxy estimates (for offline assimilations) or provided directly as 365 input to data assimilation algorithms (for online regimes). The `PSM` package facilitates all these tasks by providing users `with` modular access to commonly used proxy system forward models. The actual implementation of proxy system models is beyond the scope of DASH; instead, the `PSM` package acts as a bridge to shuttle information contained with the state vector ensemble into established proxy model codes. DASH currently supports multivariate linear models (see Hakim et al., 2016; Tardif et al., 2019; Zhu et al., 2020a), the Vaganov-Shashkin ‘Lite’ (~~VSL~~) tree ring model (~~Tolwinski-Ward et al., 2011~~) 370 (`VS-Lite`; [Tolwinski-Ward et al., 2011](#)), the BayWATCH suite of Bayesian foraminiferal and membrane-lipid models (Tierney and Tingley, 2014; Malevich et al., 2019; Tierney et al., 2019; Tierney and Tingley, 2018), a Palmer Drought Severity Index (PDSI) estimator (Guttman, 1991; Van der Schrier et al., 2011), and the models within the `PRYSM` Python package (Dee et al., 2015a) (Table 1). We anticipate that this list will grow with future advances in proxy system modeling.

Users can call the `download` method to automatically download selected forward models from their respective Github 375 repositories and add them to the MATLAB active path. The class then allows users to design `PSM` objects, which implement forward models for different proxy record with modular model parameters. Users then indicate which state vector rows hold the data needed to run each forward model; this search is facilitated by the `ensembleMetadata` class detailed in the next paragraph. Users can then ~~either~~ use the `estimate` command to run the forward models over the state vector ensemble and generate proxy estimates. Users can also run the forward models over updated state vector ensembles, in order to validate proxy 380 records against assimilation results (e.g. Tardif et al., 2019; Tierney et al., 2020b; King et al., 2021; Osman et al., 2021).

The process of running forward models on a state vector ensemble is facilitated by the `ensembleMetadata` class. This class implements objects that organize metadata along the rows and columns of a state vector ensemble. An `ensembleMetadata` object is created whenever a user builds a state vector ensemble and can also be returned for `.ens` files and `stateVector` objects. The class can be used to locate state vector rows corresponding to particular variables, spatial locations, or time sequences, and can also be used to locate specific ensemble members. A major task of `ensembleMetadata` is to locate state vector rows that correspond to proxy forward model inputs. In addition to locating specific climate variables, the class can determine which data elements are geographically closest to the location of a proxy site, which is often necessary when implementing forward models. Each `ensembleMetadata` object also holds the metadata necessary to reshape state vectors back into gridded datasets. Consequently, the class is also used to reshape DA outputs back into spatial grids for post-processing and visualization.

3.2.4 Data Assimilation Algorithms: `kalmanFilter`, `particleFilter`, `optimalSensor`

This section describes the classes used to implement data assimilation algorithms. Each class implements objects that hold parameters for a particular type of analysis. The object-oriented layout allows users to specify diverse algorithm parameters, while promoting the readability of analysis codes. Broadly, each class shares a similar usage syntax. Users first initialize an object for the desired algorithm and next provide required parameters. Here, required parameters typically include a state vector ensemble (X_p), proxy records (Y), proxy estimates (\hat{Y}) or forward models, and proxy error-variances or covariances (R). Users can specify any additional parameters, and then implement the algorithm using the `run` method. To support the use of large state vector ensembles, all three DA algorithms included in DASH are optimized for both speed and efficient use of memory.

The `kalmanFilter` class contains options for offline regimes, and may also be adapted into online frameworks. The class implements an ensemble square-root Kalman filter (Andrews, 1968), which processes ensemble means and deviations separately. This separation precludes the need for perturbed observations (Whitaker and Hamill, 2002) and provides several opportunities for enhanced computational efficiency. For example, exploratory analyses can choose to only assimilate the ensemble mean, which is significantly faster than updating the full ensemble. Other optimizations leverage the independence of deviation updates from the proxy records to minimize the number of computations of the Kalman Gain. Unlike some Kalman filter codes, DASH does not process proxy records sequentially. Instead, all records are processed simultaneously, which we refer to as a “block update”. Block updates afford several advantages over sequential processing: they are typically faster on modern computer architectures, their results do not depend on the order in which proxy records are assimilated, and they permit the use of full error-covariance matrices for R. By contrast, sequential processing only permits the use of independent error-variances, and the final results will vary with the order of the proxies when using non-linear forward models.

The `kalmanFilter` class ~~also~~ supports several methods commonly used to adjust Kalman filter covariance matrices (the $\text{cov}(X, \hat{Y}) \text{cov}(X, \hat{Y})$ term in Equation 6); these include covariance inflation (Anderson and Anderson, 1999), localization (Hamill et al., 2001), and blending ensemble covariances with a second covariance matrix (e.g. Valler et al., 2019). The class also permits user-specified covariance matrices, which can be useful when climate-system covariances are poorly defined, such

415 as for changing continental configurations in deep-time assimilations. Finally, the `kalmanFilter` class supports the use of evolving offline priors (e.g. Franke et al., 2020; Osman et al., 2021), which can be used simulate changing climate system boundary conditions while minimizing computational cost.

Naïve Kalman filter algorithms return an entire state vector ensemble in each assimilated time step, which can rapidly exceed computer memory. Consequently, the `kalmanFilter` class includes many options for reducing the size of the outputs. 420 Alternatives to saving full ensembles include only returning the ensemble mean, returning the ensemble mean and variance, and returning several percentiles of the full ensemble. The class also provides support for reconstructing climate indices from assimilated spatial fields while conserving computer memory. In many cases, an assimilated spatial field is primarily used to calculate a reconstructed climate index. The full posterior of a climate index is often useful for uncertainty analysis, but spatial fields are often too large to allow the return of full posterior ensembles. To remedy this situation, the `index` method allows 425 users to calculate and return the full posterior of a climate index (such as global mean temperature or the Nino 3.4 index), without saving the full-field posterior ensemble. We also reiterate that users can use the `ensemble` class to only assimilate a subset of the variables in a state vector. Some variables might only be necessary to run the PSMs, and excluding these variables from the algorithm can improve both memory use and run time.

The `particleFilter` class provides an alternative algorithm to Kalman filtering. In DASH, this algorithm proceeds 430 by weighting the state vectors (i.e. particles) in an ensemble and then computing a weighted mean across the ensemble. The primary option in the `particleFilter` class concerns the method used to determine the weights for the mean. By default, the class implements a Bayesian weighting scheme that conforms to a classical particle filter (see Van Leeuwen, 2009). However, users can instead choose to take a mean of the best N particles, with the number of particles specified by the user.

The `optimalSensor` class is based on the method described by Comboul et al. (2015), which is derived from an ensemble 435 Kalman filter framework. Rather than reconstructing climate variables over time, the algorithm instead tests the ability of a proxy record to reduce the variance of a climate metric calculated over an ensemble. Essentially, this method assesses the relative influence of individual proxy records on a reconstructed index (such as a spatial temperature mean or climate mode index). The `optimalSensor` class provides three distinct, yet related, routines to support these types of analyses. The `evaluate` routine allows users to assess each proxy's individual ability to reduce variance in the posterior ensemble. The 440 `run` routine implements the greedy algorithm of Comboul et al. (2015), and allows users to rank the utility of proxy sites for successive assimilation. Finally the `update` routine assesses the total variance reduced by an entire proxy network. These commands can also be combined to examine changes in proxy influence as additional records are added to a network.

~~Classically, the The classical optimal sensor algorithm strictly relies on sequential processing and so requires proxy error-variances, which necessarily . Thus, the classical algorithm assumes that assimilated proxy records are independent. However, 445 the optimalSensorupdate class extends the algorithm to allow for method uses a block update to process the proxy network, and so also permits the use of covarying proxy errors. In this case, the covarying proxies are processed using a single block-update, effectively treating the covarying proxies Essentially, the entire network is treated as a single sensor, and the routine calculates the total variance reduced by this network. This is useful when assimilating assessing the variance reduced~~

450 by gridded, spatially-covarying proxy networks and climate field reconstructions (e.g. King et al., 2023), such as drought atlases (e.g. Cook et al., 1999, 2010; Morales et al., 2020).

4 Examples

In this section, we provide two examples illustrating the use of the DASH toolbox. These examples are designed to demonstrate the utility of DASH for a variety of analyses over different spatial scales, time periods, and proxy networks. These examples closely mimic several existing studies in the paleoclimate DA literature (King et al., 2021; Tierney et al., 2020b; Osman et al., 455 2021), although we have modified the analyses at several points for brevity or to demonstrate the extended capabilities of the DASH toolbox. Numbers in parentheses refer to the line numbers in the code for each example.

4.1 Northern Hemisphere Summer Temperatures over the Last Millennium

Our first example illustrates a possible setup for reconstructing summer temperatures in the extratropical Northern Hemisphere over the last millennium using annually resolved proxies. This example follows the assimilations found in King et al. (2021), 460 although for the sake of simplicity, we only assimilate a single climate model here. In this example, we integrate a network of 54 temperature-sensitive tree-ring records (Wilson et al., 2016; Anchukaitis et al., 2017) with output from the CESM1.1 Last Millennium Ensemble (LME; Otto-Bliesner et al., 2016) to reconstruct both a summer (JJA) temperature spatial field and a spatial-mean index. We generate proxy record estimates using simple linear forward models trained on the mean temperature of each site's optimal growing season. We run the assimilation using an ensemble Kalman ~~Filter~~filter with a stationary offline 465 prior. We also apply covariance localization for the spatial field, which we implement using a Gaspari-Cohn 2D polynomial (Gaspari and Cohn, 1999) with a 20,000 km cutoff radius. Finally, we use an optimal sensor analysis to evaluate the potential influence of each tree-ring record in the network. The results of the analysis are displayed (Figure 3) using the visualization codes in the data repository.

4.1.1 Organize Climate Data

470 The first two sections of the example (lines 6-50) illustrate using `gridfile` to organize data used in the assimilation. Here, these data consist of (1) climate model output from the CESM1.1 LME and (2) tree-ring chronologies. The climate model output contains reference height temperatures from fully-forced run #2. This output is stored across two NetCDF files and spans a 2D spatial grid over the period 850 to 2005 CE at monthly resolution. Our first step is to create a metadata object that defines the scope of this dataset (lines 12-18). Here, we choose to define spatial metadata using the latitude and longitude 475 values stored in the NetCDF output files (lines 13-14). However, the time metadata in the NetCDF files is reported as “days since January 1, 850”, which is non-intuitive for our purposes. Instead, we choose to define time metadata using MATLAB’s built-in `datetime` format, which will allow us to sort time points by months and years (line 15). We also include two optional metadata attributes (the units and climate model associated with the output) to better document the dataset (line 18). We next create a `gridfile` object whose scope is defined by this metadata (line 21) and add the temperature dataset, stored

480 in the `TREFHT` variable of the two NetCDF files, to the `gridfile` object's catalogue (lines 28-29). Finally, we apply a data transformation to the catalogue (line 32) so that loaded temperature data will be returned in units of degrees Celsius, rather than Kelvin.

485 In the next section (lines 35-50), we catalogue the tree-ring chronologies. These records are stored in a binary MAT-file (line 38), along with information about each proxy site. The proxy record dataset is a 2D array that spans 54 proxy sites over time at annual resolution. Here, we choose to define metadata (line 43) along the proxy-site dimension using the ID, spatial location, and optimal growing season of each site (line 42). For time metadata, we use the calendar year corresponding to each measurement (line 43). We next create a `gridfile` object whose scope is defined by this metadata (line 46) and add the proxy record dataset, stored in the `crn` variable of the MAT-file, to the `gridfile` catalogue (line 47). Finally, we indicate that -999 values in the dataset represent fill values and should be converted to `NaN` when loaded (line 50).

490 **4.1.2 Build a State Vector Ensemble**

In the next section (line 53-96), we use the `stateVector` class to design and build a state vector ensemble. We begin by initializing and labeling a `stateVector` object (line 56), and then initializing variables within that state vector (lines 62-63). Typically, a state vector will include any variables required to run the proxy system forward models, as well as reconstruction targets. In this example, each proxy system model requires a seasonal temperature mean from the model grid point closest to 495 the proxy site. Thus, we first initialize variables for the temperature means of the proxy records using a different name for each site (line 62). We also create variables for the reconstructed spatial temperature field, and the spatial-mean index (line 63), for a total of 56 variables. All of these variables will be constructed from the monthly LME temperature output, which is indicated by the second input in lines 62 and 63. Note that the names of state vector variables do not need to match the names of variables stored in data source files – here, `TREHFT` – because multiple state vector variables may be derived from the same dataset.

500 We next specify how to select ensemble members in the state vector ensemble. In this example, we indicate that ensemble members should be selected along the time dimension, with each ensemble member associated with a particular calendar year (line 69). Using -1 as the first input applies this setting to every variable in the state vector. Here, we use January as a reference point for each calendar year, but this does not imply that the variables will necessarily contain data from the month of January. Instead, the January months are used to align variables so that the values within any given ensemble member correspond to 505 the same year. For example, consider two variables implementing seasonal means. One variable, `MJJA`, implements a seasonal mean from May to August. The other variable, `ON`, implements a seasonal mean from October to November. Although the two variables cover different seasonal windows, the seasonal windows for each ensemble member should be drawn from the same year. Here, the January reference point ensures that these seasonal windows are aligned to the same year; essentially, the variables for each ensemble member will be built using the appropriate seasonal window as indexed from the associated 510 January reference point. For an ensemble member that uses January 1850 as a reference point, the `MJJA` variable will be built using data from May-August 1850, and the `ON` variable will be built using data from October-November 1850. Although the two variables use different temporal spans, they collectively refer to the same year within the ensemble member. Additionally, the state vector class will ensure that ensemble members are only selected from years that include complete temporal spans for

all variables. Continuing the example: if the temperature dataset ended in October 1900, then 1900 will never be selected as
515 an ensemble member because the ON variable would be missing data from November of that year. We note that users are not confined to a given calendar year, as the months used in the seasonal window are indexed from the associated reference point. For example, a user could implement a DJF seasonal mean by providing indices [-1 0 1], thereby creating a seasonal window from the three monthly time steps centered on each January.

Finally, we design the variables so that each uses values from the appropriate subset of the monthly temperature dataset. For
520 the reconstruction targets, we use grid points from the extratropical Northern Hemisphere (line 78) and summer (June-August) seasonal temperature means (line 79). We note that the third input in line 78 is left empty because the latitude dimension should not be used to select different ensemble members (contrast this with the time dimension in line 69). To implement the seasonal means, we provide the indices of months relative to each January reference point. As the reference point, each January is given a relative index of 0; hence, a June-August mean is calculated using data values 5, 6, and 7 (monthly) time
525 steps after each January reference point. We also specify a latitude-weighted spatial mean for the spatial-mean index (line 80). Before designing the forward-model variables, we first note that each variable uses a different seasonal average. Including the full spatial field for multiple different seasonal windows would result in an unnecessarily large state vector, so we first use the `closest.latlon` utility to locate the model grid point closest to each proxy site (line 86). We then design each forward-model variable to consist of the site-specific seasonal temperature mean at that single grid point (lines 87-93). At this point, we
530 have finished designing the state vector, and proceed to build an ensemble with ~~1000~~1156 members (line 96). In this example, we save the built ensemble to a `.ens` file. Although the `stateVector` class can also return ensemble directly as output, we generally recommend saving to file, because this allows the DASH toolbox to use computer memory more efficiently.

4.1.3 Proxy Forward Models

The next section (lines 99-118) uses the `PSM` package and `ensembleMetadata` class to design proxy forward models and
535 run the models on values stored in the state vector ensemble. The outputs of these forward models are the proxy estimates used to compare state vector ensemble members to observed proxy records in assimilation algorithms. We begin by using the `PSM` package to create simple, linear forward models for each proxy site (line 109). The coefficients for each model are calibrated to mean temperature over the optimal growing season at each proxy site. Determining forward model coefficients is beyond the scope of this example, but King et al. (2021) compute these values by regressing the proxy records against an instrumental
540 temperature dataset. After designing each model, we next indicate the state vector row that corresponds to the inputs for each model (lines 113-114). Finally, we use the `estimate` command to run the forward models on the ensemble and generate the proxy estimates (line 118).

4.1.4 Kalman Filter

In this section (lines 121-174), we use the `kalmanFilter` class to implement an ensemble Kalman filter and reconstruct
545 summer temperatures. We first initialize and label a `kalmanFilter` object, which will store the parameters used to run the assimilation (line 124). The mandatory parameters for an ensemble Kalman filter are (1) a prior ensemble, (2) proxy records, (3)

proxy estimates, and (4) proxy error covariances or variances, and we provide these parameters to the `kalmanFilter` object in lines 130, 133, 134, 135, and 139. Determining proxy error variances is beyond the scope of this example, but King et al. (2021) compute these values by running the proxy forward models on an instrumental temperature dataset and comparing the resulting proxy estimates to the real proxy records. In this example, we also implement covariance localization. To accomplish this, we first calculate localization weights for the ensemble and proxy sites (line 144) and then provide these weights as parameters to the `kalmanFilter` object (line 145).

To illustrate the flexibility of the DASH architecture, we also demonstrate a second method for reconstructing the spatial-mean summer temperature index (line 153). This method allows the user to calculate an index from the posterior of a spatial field, without saving the (often very large) spatial field posterior. To further conserve memory, we also indicate that the filter should only record the variance and percentiles of the posterior ensemble (lines 156-157), rather than the much larger full posterior. Finally, we run the Kalman filter algorithm for the analysis and return the mean, variance, and posterior mean and percentiles of the target reconstruction variables (line 160). We note that the reconstructed spatial field is organized as a state vector, but many mapping functions operate on spatial matrices, rather than vectors. Hence, to facilitate display of the reconstructed spatial field, we regrid the posterior to the spatial dimensions of the original climate model output (lines 164-165). We also extract the assimilated spatial temperature mean, which is the final element along the state vector (line 168), and the alternative spatial mean, which was calculated from the updated spatial field (line 170).

Figure 3a-c illustrates the results of this assimilation. The upper panel Panel (a) compares the reconstructed indices obtained using the two different methodologies: the blue line depicts the index obtained by assimilating the temperature spatial mean directly in the state vector, and the red line depicts the index calculated from the updated (posterior) spatial field. The lower left and lower center panels display an example. Panel (b) displays the reconstructed spatial field from 1850 CE along with an uncertainty quantification based on, and (c) illustrates the uncertainty quantification derived from the variance of the field's posterior ensemble. Notably, panel (a) demonstrates that the spatial indices calculated using the two different methods are not identical. In brief, this discrepancy occurs because (1) the index calculated from the posterior field (in red) is sensitive to spatial heterogeneity in the Kalman filter updates, and (2) the directly assimilated index (in blue) is less sensitive to the proxy records than are individual spatial sites. The causes and implications of this behavior are discussed in greater detail in Section 5.3.

4.1.5 Optimal Sensor

In the final section (lines 177-194), we use an optimal sensor framework to evaluate the influence of each proxy on the reconstructed spatial-mean index. Analogous to the `kalmanFilter` object of the previous section, here we will use an optimalSensor object to organize parameters for the analysis. The required parameters for an optimal sensor are (1) a sensor metric, (2) proxy estimates, and (3) proxy error variances or covariances. After initializing and labeling the `optimalSensor` object (line 180), we set the extratropical summer temperature index as the sensor metric (lines 183-184) and also provide proxy estimates and error-variances (lines 187-188). With these parameters set, we then use the optimal sensor to evaluate the power of each proxy for reconstructing the spatial-mean index (lines 191).

580 Figure 3(lower right) displays the results of this analysis. Here, the ability of a proxy to reduce variance responds to two factors: the covariance of its estimates with the modeled spatial-mean index, and its uncertainty values (R), which represent the accuracy of its forward model. Thus, the proxies with the greatest ability to reduce variance are characterized by more accurate forward models and stronger covariance with the spatial-mean index.

4.2 Global Sea Level Pressures at the Last Glacial Maximum

585 Our second example illustrates a setup for reconstructing global sea level pressures from the Last Glacial Maximum (LGM) to present. This example is inspired by Osman et al. (2021) with several modifications. First, we assimilate global sea level pressures rather than sea surface temperatures (SSTs) in order to demonstrate the reconstruction of climate variables not directly sensed by the proxy network. For the sake of simplicity, we also limit the proxy network to the alkenone $U_{37}^{K'}$ and $\delta^{18}\text{O}$ of planktic foraminifera SST proxies, neglect spatial variations in proxy seasonal sensitivities, and reconstruct spatial fields on a
590 3,000-year time step. In this example, we integrate a network of $U_{37}^{K'}$ and $\delta^{18}\text{O}$ sediment records with output from the isotope-enabled Community Earth System Model (iCESM1.2; Brady et al., 2019; Tierney et al., 2020b; Zhu et al., 2017; Stevenson et al., 2019). We generate proxy record estimates using the BayFOX (Malevich et al., 2019) and BaySPLINE (Tierney and Tingley, 2018) forward models. We conduct the assimilation using an ensemble Kalman filter with an evolving offline prior and also implement a proxy-validation analysis. The results of this analysis are displayed in Figure 4 using the visualization
595 codes in the data repository.

4.2.1 Organize Climate Data

Similar to Example 1, the first two sections again use the `gridfile` package to organize climate data. Here, the data consists of (1) climate model output from iCESM binned to 50-year monthly climatologies, and (2) $U_{37}^{K'}$ and $\delta^{18}\text{O}$ proxy records. The climate model output includes variables for the sea-level pressure (SLP) reconstruction target, as well as sea surface
600 temperatures (SSTs) and $\delta^{18}\text{O}_{sw}$, which are used to run the proxy forward models. The climate variables reflect mean monthly values averaged over 50-year intervals in order to more closely match the multi-decadal averages captured by the proxy records (Tierney et al., 2020b; Osman et al., 2021). This output includes sixteen 50-year averages for each of the nine 3,000-year intervals from the LGM to present, for a total of 144 possible ensemble members. The data for the variables are stored in three separate NetCDF files. The SLP variable is provided on a rectilinear atmosphere grid, and the creation of its gridfile catalogue
605 (lines 13-18, 27, 32) follows the process outlined in section 4.1.1. By contrast, the SST and $\delta^{18}\text{O}_{sw}$ variables are sourced from the ocean component of the model, which uses a tripolar coordinate system. Tripolar datasets typically include dimensions for both latitude and longitude, but spatial metadata is not fixed for any given element of either dimension. For example, the latitude value at $(\text{latitude}_j, \text{longitude}_k)$ is not the same as the latitude value for $(\text{latitude}_j, \text{longitude}_{k+1})$. Consequently, the dataset describes values at distinct (latitude, longitude) points, rather than values on a rectilinear (latitude x longitude) grid. The
610 `gridfile` class requires fixed metadata values along each data dimension, so we define the metadata for SST and $\delta^{18}\text{O}_{sw}$ using unique spatial sites (lines 20-24), rather than a rectilinear latitude x longitude format. Note on lines 33 and 34 that two dataset dimensions are associated with the site spatial dimension. This syntax merges the latitude and longitude dimensions

in the `gridfile` catalogue and treats them as a single spatial dimension. We next use `gridfile` to catalogue the proxy records (lines 37-49). Here, the proxy records are stored in a binary MAT-file, along with metadata describing the records. This
615 metadata includes the ID, spatial coordinates, proxy type ($U_{37}^{K'}$ or $\delta^{18}\text{O}$), and foraminiferal species associated with each record (line 43).

4.2.2 State Vector Ensemble and Evolving Prior

We next design and build the state vector ensemble for the LGM assimilation (lines 52-80). We begin by initializing a
620 `stateVector` object with three variables (lines 55 and 60). The first variable, `SLP`, is the reconstruction target; the other two variables, `SST` and $\delta^{18}\text{O}_{sw}$, are required to run the proxy forward models. We next indicate that ensemble members should be selected from different points in time with each ensemble member associated with a particular 50-year average and we specify January as the reference point (line 65). In this example, we target annual `SLP` values. Since we are neglecting spatial variations in proxy seasonal sensitivities, we also require annual `SST` and $\delta^{18}\text{O}_{sw}$ values as proxy forward model inputs. Thus, we use an annual mean for each of the three variables (line 69).

We note that, unlike Example 1, we do not design variables for the individual proxy records; instead, we include the entire
625 spatial field for each climate variable used by the forward models. This syntax simplifies the code but results in a larger state vector. We elect to use this syntax here in order to improve code clarity and also demonstrate the flexibility of the DASH architecture. However, other applications should compare the benefits of code clarity with greater memory use when choosing a syntax. Finally, we build a state vector ensemble using all available ensemble members (line 73). We select ensemble members
630 sequentially in order to facilitate the creation of an evolving prior. This orders the ensemble members so that the sixteen 50-year averages for each 3,000-year interval are all in succession. We next use the `evolving` command to implement an evolving prior for the different 3,000-year intervals (line 80). For this command, the columns of the `members` variable indicate which ensemble members should be used for each evolving prior. Here, each prior is built using the sixteen 50-year averages for one of the nine 3,000-year intervals.

635 4.2.3 Proxy Forward Models

We next build and run proxy forward models on the state vector ensemble in order to generate a set of proxy estimates. Here, we use the `BaySPLINE` and `BayFOX` Bayesian forward models for $U_{37}^{K'}$ and $\delta^{18}\text{O}$, respectively. We begin by using the `download` command to download the models from their respective Github repositories and add them to the MATLAB active path (lines 86-87). We next design a forward model for each proxy record using the model appropriate for each proxy's
640 type (lines 90-120). For the `BaySPLINE` model, we locate state vector rows corresponding to the `SST` values from the climate model grid point closest to each proxy record (lines 101-104). The `BayFOX` model is calibrated to different foraminiferal species, so we initialize each model with the species of the associated proxy record (line 109). We then locate both `SST` and $\delta^{18}\text{O}_{sw}$ values, again at the closest climate model grid point (lines 112-114). For the purposes of documentation, we also label each forward model with the ID of the associated proxy record (line 118). Finally, we run the forward models on the

645 evolving state vector ensemble using the `estimate` command (line 124). In addition to proxy estimates, the BaySPLINE and BayFOX models calculate proxy error-variances, provided as the second output, which we use to define `R`.

4.2.4 Kalman Filter and Proxy Validation

We next implement the Kalman ~~Filter~~filter analysis (lines 127-149). We first initialize and label a `kalmanFilter` object (line 130) and then provide the required algorithm parameters (lines 134-137). To conserve memory, we only return the mean and
650 variance of the posterior ensemble (line 141). As in Example 1, we regrid the reconstructed spatial field to the dimensions of the original climate model to support visualization and post-processing (lines 145-146; Figure 4). Unlike Example 1, we include all of the climate variables needed for the proxy forward models in the prior. This allows us to run the proxy forward models on the reconstruction and generate proxy posterior estimates. We can then compare these estimates to the real proxy records as a basic assessment of reconstruction skill (Figure 4). We implement this process by applying the `estimate` command to the
655 posterior (line 155). For the sake of brevity, we only implement a simplified proxy validation in this example. In practice, DA applications should validate the reconstruction using proxies withheld from the assimilation (e.g. Tierney et al., 2020b; Osman et al., 2021; King et al., 2021) so that assimilated proxies do not inform the skill of their own validation values.

4.3 Additional Considerations

The examples presented above touch upon many aspects of paleoclimate DA workflows but cannot be exhaustive. For the
660 sake of brevity and clarity, we have neglected several considerations common in DA applications. One particular step we have omitted is the determination of proxy uncertainties (`R` in equations 4, 6, and 7). In some cases, proxy uncertainties (`R`) may be provided by the proxy forward models (as in Example 2) or from the calibration of the forward models (e.g. Tardif et al., 2019; King et al., 2021). Another potential approach involves running the forward models on instrumental data and comparing the resulting proxy estimates to the real proxy records (e.g. King et al., 2021, 2023). However, we note that these approaches are
665 not applicable to all analyses, so users may need to develop additional methods to estimate proxy uncertainties. For example, methods that estimate proxy error-variances (e.g. Tardif et al., 2019; Tierney et al., 2020b; King et al., 2021) implicitly assume the independence of proxy uncertainties. However, this assumption may not hold when proxy records are strongly correlated or sensitive to the same local factors. When this occurs, proxy error-covariances should be used in place of error-variances (see King et al., 2023, for an example). We also discuss additional issues common to many paleoclimate applications in the ~~section~~
670 below~~following~~section.

5 Warnings and Best Practices

While it is not possible to detail all the issues that can occur when using DA for paleoclimate reconstructions, here we mention several cautions and suggestions for best practices. Along with methodological considerations, DA users should be aware of the limitations of both the proxy data and prior modeled climate states. In other words, simply running an assimilation code does
675 not guarantee that a reconstruction is scientifically valid, and potential DA users should understand the tradeoffs and limitations

of DA methods when designing a reconstruction. In this section, we present several major challenges that may be encountered in paleoclimate DA and outline approaches to mitigate or recognize their effects. This list is by no means exhaustive, and we strongly recommend that potential DASH users first familiarize themselves with the paleoclimate DA literature and also evaluate their reconstructions for sensitivity to the assumptions and input data.

680 5.1 Temporal Variability

A major issue when using an ensemble Kalman filter with a static prior (e.g. Steiger et al., 2014; Hakim et al., 2016; Dee et al., 2016; Tardif et al., 2019; Steiger et al., 2018; Neukom et al., 2019; Zhu et al., 2021a; King et al., 2021, 2023) is that the proxy network's size and composition – and changes to these properties over time – can directly alter the temporal variability of the reconstruction. Essentially, we observe that variability is artificially reduced as the proxy network becomes smaller. It 685 is common for the sample size of a proxy network to change over a reconstructed time period. When this occurs, then the variability of the reconstruction will be non-stationary and relative climate variability may not remain consistent over the span of the reconstruction.

This effect occurs because a static prior implies zero temporal variability as an *a priori* assumption in the absence of proxy information. Consider a “no-information” case, in which a static prior is assimilated with an empty proxy network. Since the 690 proxy network is empty, the prior ensemble will not receive any updates, and the reconstruction will be the mean of the prior in every time step. Since the prior is identical in every time step, the reconstruction will consist of a constant value over time and will exhibit no temporal variability. With the addition of a proxy record to the network, the prior will begin to receive updates, and the reconstruction will begin to gain temporal variability. Each subsequent record added to the proxy network increases the ability of the method to move the reconstruction away from the prior mean, and so reconstruction variability will increase with 695 the size of the proxy network. This behavior is by design: in the absence of additional information, the prior provides the best estimate of the mean state of the climate system. However, it creates complications for paleoclimate interpretations. We note that this effect is most severe for smaller proxy networks and at spatial points informed by a limited number of proxy records.

Because of this effect, it is essential that assimilations using static priors account for the effects of proxy network composition on temporal variability. Variance adjustment methods are common in other approaches to paleoclimate reconstruction 700 (e.g. Cook et al., 1999; Esper et al., 2005; Frank et al., 2007; Anchukaitis et al., 2017), and King et al. (2023) provide an example for how this can be accomplished for DA applications. [However, there is no simple fix for the variance loss issue, and we note that variance adjustment methods will raise the uncertainties of reconstructed values.](#) Alternatively, evolving priors can mitigate the variance [loss](#) issue (e.g. Tierney et al., 2020b; Osman et al., 2021) by removing the *a priori* assumption of zero temporal variability. However, we caution that evolving priors could still exhibit a variance dampening effect when the 705 variability between reconstruction time steps and the state of the evolving priors is dominated by internal climate variability.

5.2 Climate model biases

A second major concern for paleoclimate DA concerns the effects of climate model biases on assimilated reconstructions. In this discussion, we find it useful to distinguish between (1) biases in the mean state, and (2) climate model covariance biases.

Mean state bias refers to the systematic tendency of a simulated variable to be too high or too low compared to observations.

710 Covariance bias refers to errors in the linear relationship between climate variables at different spatial points, or between different variables. Essentially, these are biases in the teleconnection patterns associated with various climate phenomena. Since the model prior covariance determines how information propagates from a proxy network to ~~distal~~distant parts of a climate field, differences between the real and modeled climate system covariance will cause errors in the assimilation. No climate model can ~~match the complexity of represent~~ the real Earth system with complete accuracy and so all climate models
715 necessarily include some degree of error.

An additional consequence of climate model biases concerns method testing and proof-of-concept studies for paleoclimate DA. Typically, these studies rely on pseudo-proxy frameworks (Smerdon, 2012), in which climate model output is used to simulate a set of proxy records. These pseudo-proxy records are designed to mimic a real proxy network and can be used to reconstruct the climate model output. Unlike the real past climate history, the climate model output is fully
720 known and so these experiments provide an opportunity to assess assimilation skill. Due to the complexity of skill assessments, it can be tempting to use the same climate model to both generate the pseudo-proxies and build the assimilation prior. However, we caution that this framework represents an unrealistic “perfect-model” design, in which the climate model used for assimilation perfectly describes the target climate system. Although perfect-model experiments have their uses, climate model biases represent a major source of error in paleoclimate DA (Dee et al., 2016; King et al., 2021)
725 (Dee et al., 2016; Amrhein et al., 2020; King et al., 2021) and DA users should account for these biases to accurately quantify DA skill. Ultimately, “biased-model” experiments, which use different climate models to generate pseudo-proxies and build the assimilation prior, are necessary for accurate method testing. We also note that the exact nature of climate model biases will vary by the choice of model and the specific target climate variable(s), and so an ensemble of different biased-model tests is often necessary to capture the full effects of climate model biases.

730 Deleterious effects in real assimilations also occur when the inputs to the proxy forward models exhibit mean state biases. For example, consider using the VS-Lite tree-ring model (Tolwinski-Ward et al., 2011) to assimilate a climate model with a persistent cold bias. VS-Lite includes a temperature threshold based on absolute Celsius units; at temperatures below this threshold, VS-Lite ~~assume~~assumes no growth occurs and produces a proxy estimate of zero. As a result, a climate model with a cold bias may consistently fall below this threshold, causing VS-Lite to estimate a null proxy record. In this case,
735 as a consequence of the mean state bias in the climate model, VS-Lite would assume that trees cannot grow at a location where they do grow in reality, and this error would degrade the reconstruction. More generally, mean state biases propagate through the forward models to the proxy estimates and thereby influence the comparison of the ensemble members to the real proxy records. In some cases, these biases can cause artificial trends in a reconstruction. Essentially, the assimilation draws reconstructed variables unilaterally in the direction of less biased mean values. Although this does indeed improve the
740 final estimate of a variable’s value, this behavior is mixed with the variable’s reconstructed temporal evolution and causes an artificial trend.

Some mean state biases can be addressed by the process of bias correction used in other disciplines and applications (e.g. Wang and Robertson (2011); Zhao et al. (2017); Cannon et al. (2015); Cannon (2018); Galmarini et al. (2019), and see Steiger

et al. (2018) for a DA example). When appropriate, users can alternatively avoid the effects of mean state biases by providing
745 climate anomalies to the proxy forward models, rather than absolute values (e.g. Tardif et al., 2019; King et al., 2021, 2023). This is often appropriate for assimilations that rely on linear proxy forward models or forward models not dependent on absolute units. If using priors from multiple climate models, users may also need to avoid or account for time periods when climate models strongly differ, as strongly differing climate representations can act analogously to mean state biases. For example, the instrumental era is often not suitable for computing climate model anomalies for long preindustrial and last millennium
750 simulations, because the climate response to recent anthropogenic influences can vary across models during the relatively short historical period. By contrast, anomalies assessed relative to the entire pre-industrial period are typically more stable.

Covariance biases are perhaps the more challenging issue to deal with since they bias the propagation of information from the proxy records to the reconstruction targets and do not present simple fixes. Multivariate bias correction methods may provide a solution to this issue (e.g. Cannon, 2018; Vrac, 2018; Galmarini et al., 2019), but these methods have thus far seen
755 little use in paleoclimate DA contexts. Instead, a more common solution is to assimilate a multi-model ensemble (Parsons et al., 2021; King et al., 2021, 2023). Users may enact this using a single multi-model prior (e.g. Parsons et al., 2021; King et al., 2023), or by performing an ensemble of assimilations using different single-model priors (e.g. King et al., 2021). When possible, we recommend the use of multi-model priors. These priors are supported in the DASH framework, and they limit the effects of covariance biases by down-weighting covariance patterns that disagree across different models. We also note that
760 this down-weighting may in part contribute to spatial heterogeneity in Kalman filter updates, which we discuss in detail in the next section.

5.3 Physically inconsistent reconstructions

Both the particle filter and Kalman filter frameworks assume that all state vector variables and proxy estimates follow a Gaussian distribution; however, not all climate variables meet this criterion. Thus, DA users should take care to transform non-
765 Gaussian variables into an approximately Gaussian space before assimilation. Failing to take this step can result in unrealistic or nonphysical reconstructed values. This is often relevant when assimilating variables distributed near the lower bounds of their domains. For example, precipitation variables typically have a high probability near zero, yet cannot fall below zero, and this results in a strongly non-Gaussian distribution. Because of this, raw precipitation values are not suitable for assimilation and using them can cause the method to return non-physical negative precipitation values. Users should therefore transform
770 precipitation into an approximately Gaussian shape before assimilation. The reverse transformation can then be applied to the assimilated variables in order to obtain reconstructed precipitation. Possible transforms for variables near a lower bound include the extended Box-Cox and log transforms (Wang et al., 2012), and the logit transform may be appropriate for variables on a finite interval (such as any variable that represents a percentage). Ultimately though, the most appropriate transforms will vary by application (Wang et al., 2012).

775 We also emphasize that the DA algorithms described in this paper do not conserve physical properties like mass or energy. Consequently, assimilated reconstructions are not bound by the governing equations inherent to the climate models used to generate a prior ensemble and can produce physically inconsistent values. In some cases, this may mean that assimilated fields

are not suitable for providing boundary conditions for climate model simulations. Unrealistic values can also arise when individual proxy records are given excessive weight in the Kalman filter. When the magnitudes of proxy weights are too large, 780 small proxy innovations can result in drastically large updates to assimilated climate variables. This issue most commonly occurs when proxy uncertainties (R) are severely underestimated. For example, in Example 1 our proxy uncertainties incorporate both forward-model errors and non-climatic noise in the proxy records. However, if we neglect these effects and compute R using only the uncertainties inherent in measuring tree-ring variables (which are vanishingly small), the resulting Kalman filter updates alter the assimilated temperature field by thousands of degrees Kelvin, a clearly unrealistic result. This behavior underscores the importance of correctly incorporating multiple sources of error when quantifying proxy uncertainties. Although We also note that DA methods that conserve physical properties do exist; for example, adjoint approaches are often used in paleoceanography to conserve physical properties in the ocean (e.g. Winguth et al., 2000; Kurahashi-Nakamura et al., 2014; Dail and Wunsch, 2015). However, these methods have seen little use in paleoclimate—are less common outside of paleoceanographic contexts, likely due to the prevalence and lower computational cost of offline configurations.

790 A related issue concerns the spatial heterogeneity of Kalman filter updates, which can also result in physically inconsistent behavior. When assimilating spatial climate fields, the magnitudes of Kalman filter updates often vary unevenly across different spatial points. The magnitude of the update at a given spatial point is proportional to that point's covariance with the proxy estimates, so distant spatial points that covary less strongly with the proxy network will receive smaller updates. As a result, reconstructed values at distant sites tend to remain closer to the prior ensemble mean and exhibit lower temporal variability 795 than sites closer to the proxy network. This lower variability is not a real climate phenomenon, but rather a consequence of the Kalman filter method, which is designed to estimate mean states rather than temporal variability. However, we also note that the variance of the posterior ensemble is available for users to assess the uncertainty resulting from smaller updates.

This spatial heterogeneity also has consequences for reconstructing large-scale climate indices, such as those used to characterize first-order climate modes and spatial averages. These indices are typically computed using values from multiple points 800 in a spatial climate field; however, the uneven application of Kalman Filter~~filter~~ updates to different spatial points can skew the calculation of these indices. For example, consider the Southern Annular Mode (SAM): one index commonly used to measure the SAM's phase is defined using the gradient of zonal mean sea level pressures between 40°S and 65°S (Gong and Wang, 1999). Consider an assimilation that uses a proxy network primarily located near 65°S. Because of the location of the proxy network, spatial points near 65°S will receive larger updates than those near 40°S; by contrast, points near 40°S will be less 805 altered and will remain close to the mean of the prior. As a consequence of this effect, a SAM index determined from the posterior spatial field using this network might only reflect changes to values at 65°S, thereby failing to assess changes at the northern end of the gradient. Thus, when reconstructing climate indices from posterior spatial fields, it is essential for DA users to demonstrate the homogeneity of update magnitudes at the spatial points used to calculate propagate the uncertainties of the utilized grid cells into the overall uncertainty of the index. An alternative approach to reconstructing climate indices 810 is to include the climate index directly in the state vector, which precludes the issue of spatial heterogeneity. A tradeoff of this approach is that proxy records will covary less strongly with large-scale indices than with local climate variables, and so

reconstruction uncertainty may remain higher overall. However, in the case of spatial heterogeneity, we emphasize that higher uncertainties are preferable to a physically implausible reconstruction.

6 Past Applications and Future Development

815 Because of its flexibility, earlier versions of the DASH toolbox have already been used to implement several paleoclimate reconstructions, ranging across a variety of time scales and reconstruction targets. Tierney et al. (2020b) used a DASH prototype to reconstruct global temperatures at the Last Glacial Maximum using a large proxy network of geochemical SST proxies and model output from iCESM1.2. King et al. (2021) used the toolbox to reconstruct summer temperatures in the extratropical Northern Hemisphere over the last millennium by integrating a temperature-sensitive tree ring network with an ensemble of 820 climate model simulations. Osman et al. (2021) used DASH to produce a full-field reconstruction of surface temperatures from the Last Glacial Maximum to present. Rather than conducting a field reconstruction, King et al. (2023) targeted a climate mode index and reconstructed the Southern Annular Mode over the Common Era using a southern hemisphere proxy network, drought atlases, and a multi-model ensemble. In a deep-time application, Tierney et al. (2022) used DASH to produce a temperature field reconstruction of the Paleocene-Eocene Thermal Maximum. In all of these studies, DASH was used to 825 implement the assimilation workflow.

DASH is an active project and we anticipate continued developments to the toolbox. Currently, we have three major areas of focus for future improvement. First, we note that proxy system modeling is an area of active research. We anticipate the development of new proxy models and recognize the need to incorporate these future models into the DASH framework. Thus, we are continuing to expand the PSM package to include a more diverse array of published forward models. Furthermore, DASH 830 includes templates for adding proxy forward models, thereby allowing users to incorporate new models into the toolbox as the need arises. Second, we intend to expand DASH's support of online assimilation algorithms. DASH has primarily been used to implement offline assimilation regimes, and this has influenced the development of the toolbox. We note that DASH already provides a scaffold for online assimilations, as the routines in the toolbox can be used to update climate model output before reinitializing a climate model externally. However, future development will include adding explicit wrappers to commonly used 835 Earth system emulators and models of varying complexity. For example, SPEEDY-IER (Dee et al., 2015b) and linear inverse models (Perkins and Hakim, 2020) have been used to implement assimilations, and both are targets for further development of DASH. Third, we recognize that DASH's reliance on MATLAB precludes a fully open-source toolbox. Although the source code for DASH is public, the toolbox will not be accessible to users lacking a MATLAB license. Consequently, long term we aim to port the toolbox to a native Python and/or Julia package.

840 7 Conclusions

In this paper, we describe the features and foundations of DASH, a MATLAB toolbox supporting paleoclimate data assimilation. The toolbox is designed for scripting and command-line use and helps implement common tasks in paleoclimate data

assimilation workflows. Broadly, these include integrating data stored in different formats, designing state vector ensembles, running proxy system forward models, and implementing computationally-efficient data assimilation algorithms. The toolbox
845 provides an interface for external, proxy-system models commonly used in the paleoclimate literature. Data assimilation algorithms in the toolbox include ensemble Kalman filters (both offline and online regimes), particle filters, and optimal sensor analyses. The package is highly flexible and is designed for general paleoclimate data assimilation, rather than any particular DA analysis. As a result of this flexibility, DASH has already been used to implement published paleoclimate reconstructions for a variety of time scales, spatial regions, and proxy networks.

850 *Code and data availability.* Releases of the DASH toolbox are available on DASH's Github repository (<https://github.com/JonKing93/DASH/releases>), on MATLAB FileExchange (<https://www.mathworks.com/matlabcentral/fileexchange/120453-dash>), and in the MATLAB Add-On Explorer. The DASH source code is also available on the Github repository (<https://github.com/JonKing93/DASH>). The input data sets, DASH 4.2.0 release, and visualization codes used in the examples of this paper are available in a public Zenodo repository (<https://zenodo.org/record/7545722>).

855 *Author contributions.* J.K. wrote the source code for the DASH toolbox. Program conceptualization, the feature set, and the overarching research goals were developed by J.K., K.J.A. and J.E.T. All authors tested the toolbox, suggested additional features and improvements, and provided feedback on implementation, documentation, and tutorials. J.K. and M.O. designed the usage examples. All authors wrote the paper.

Competing interests. The authors declare no competing interests.

860 *Acknowledgements.* We thank Jessica Badgeley, Steven Malevich, and Feng Zhu for testing early versions of DASH, suggesting features, and for fruitful discussions about implementing paleoclimate data assimilation. We also thank Dave Meko, Sylvia Dee, and Suz Tolwinski-Ward for developing and publishing proxy forward model codes used by DASH. We thank the NCAR modeling group for producing and publishing climate model output used in our examples. The development of DASH was supported by grants from the US National Science Foundation (AGS-1803946, to K.J.A.), grant 2016-015 from the Heising-Simons Foundation (to J.E.T.), and the David and Lucile Packard
865 Foundation (to J.E.T.).

References

Acevedo, W., Fallah, B., Reich, S., and Cubasch, U.: Assimilation of pseudo-tree-ring-width observations into an atmospheric general circulation model, *Climate of the Past*, 13, 545–557, 2017.

Alley, R. B.: Palaeoclimatic insights into future climate challenges, *Philosophical Transactions of the Royal Society of London. Series A: Mathematical, Physical and Engineering Sciences*, 361, 1831–1849, 2003.

Amrhein, D. E., Wunsch, C., Marchal, O., and Forget, G.: A global glacial ocean state estimate constrained by upper-ocean temperature proxies, *Journal of Climate*, 31, 8059–8079, 2018.

Amrhein, D. E., Hakim, G. J., and Parsons, L. A.: Quantifying structural uncertainty in paleoclimate data assimilation with an application to the last millennium, *Geophysical Research Letters*, 47, e2020GL090485, 2020.

Anchukaitis, K. J., Wilson, R., Briffa, K. R., Büntgen, U., Cook, E. R., D'Arrigo, R., Davi, N., Esper, J., Frank, D., Gunnarson, B. E., et al.: Last millennium Northern Hemisphere summer temperatures from tree rings: Part II, spatially resolved reconstructions, *Quaternary Science Reviews*, 163, 1–22, 2017.

Anchukaitis, K. J., Cook, E. R., Cook, B. I., Pearl, J., D'Arrigo, R., and Wilson, R.: Coupled Modes of North Atlantic Ocean-Atmosphere Variability and the Onset of the Little Ice Age, *Geophysical research letters*, 46, 12417–12426, 2019.

Anderson, J. L. and Anderson, S. L.: A Monte Carlo implementation of the nonlinear filtering problem to produce ensemble assimilations and forecasts, *Monthly weather review*, 127, 2741–2758, 1999.

Andrews, A.: A square root formulation of the Kalman covariance equations., *AIAA Journal*, 6, 1165–1166, 1968.

Ault, T., Deser, C., Newman, M., and Emile-Geay, J.: Characterizing decadal to centennial variability in the equatorial Pacific during the last millennium, *Geophysical Research Letters*, 40, 3450–3456, 2013.

Ault, T. R., Cole, J. E., Overpeck, J. T., Pederson, G. T., and Meko, D. M.: Assessing the risk of persistent drought using climate model simulations and paleoclimate data, *Journal of Climate*, 27, 7529–7549, 2014.

Bhend, J., Franke, J., Folini, D., Wild, M., and Brönnimann, S.: An ensemble-based approach to climate reconstructions, *Climate of the Past*, 8, 963–976, 2012.

Bradley, R. S.: Are there optimum sites for global paleo-temperature reconstructions?, in: *Climatic Variations and Forcing Mechanisms of the Last 2000 Years*, edited by P. D. Jones, R. S. B. and Jouzel, J., vol. 41 of *NATO ASI*, pp. 603– 624, Springer-Verlag, New York, 1996.

Brady, E., Stevenson, S., Bailey, D., Liu, Z., Noone, D., Nusbaumer, J., Otto-Bliesner, B., Tabor, C., Tomas, R., Wong, T., et al.: The connected isotopic water cycle in the Community Earth System Model version 1, *Journal of Advances in Modeling Earth Systems*, 11, 2547–2566, 2019.

Burke, K. D., Williams, J. W., Chandler, M. A., Haywood, A. M., Lunt, D. J., and Otto-Bliesner, B. L.: Pliocene and Eocene provide best analogs for near-future climates, *Proceedings of the National Academy of Sciences*, 115, 13 288–13 293, 2018.

Cane, M. A., Braconnot, P., Clement, A., Gildor, H., Joussaume, S., Kageyama, M., Khodri, M., Paillard, D., Tett, S., and Zorita, E.: Progress in paleoclimate modeling, *Journal of Climate*, 19, 5031–5057, 2006.

Cannon, A. J.: Multivariate quantile mapping bias correction: an N-dimensional probability density function transform for climate model simulations of multiple variables, *Climate dynamics*, 50, 31–49, 2018.

Cannon, A. J., Sobie, S. R., and Murdock, T. Q.: Bias correction of GCM precipitation by quantile mapping: how well do methods preserve changes in quantiles and extremes?, *Journal of Climate*, 28, 6938–6959, 2015.

Chen, Z. et al.: Bayesian filtering: From Kalman filters to particle filters, and beyond, *Statistics*, 182, 1–69, 2003.

Coats, S., Smerdon, J., Stevenson, S., Fasullo, J., Otto-Bliesner, B., and Ault, T.: Paleoclimate constraints on the spatiotemporal character of past and future droughts, *Journal of Climate*, 33, 9883–9903, 2020.

905 Comboul, M., Emile-Geay, J., Hakim, G. J., and Evans, M. N.: Paleoclimate Sampling as a Sensor Placement Problem, *Journal of Climate*, 28, 7717–7740, <https://doi.org/10.1175/JCLI-D-14-00802.1>, 2015.

Cook, B. I., Cook, E. R., Anchukaitis, K. J., Seager, R., and Miller, R. L.: Forced and unforced variability of twentieth century North American droughts and pluvials, *Climate dynamics*, 37, 1097–1110, 2011.

Cook, E. R., Meko, D. M., Stahle, D. W., and Cleaveland, M. K.: Drought reconstructions for the continental United States, *Journal of Climate*, 12, 1145–1162, 1999.

910 Cook, E. R., Anchukaitis, K. J., Buckley, B. M., D'Arrigo, R. D., Jacoby, G. C., and Wright, W. E.: Asian monsoon failure and megadrought during the last millennium, *Science*, 328, 486–489, 2010.

Crowley, T. J.: Utilization of paleoclimate results to validate projections of a future greenhouse warming, in: *Developments in atmospheric science*, vol. 19, pp. 35–45, Elsevier, 1991.

915 Dail, H. and Wunsch, C.: Dynamical reconstruction of upper-ocean conditions in the Last Glacial Maximum Atlantic, *Journal of climate*, 27, 807–823, 2014.

Dee, S., Emile-Geay, J., Evans, M., Allam, A., Steig, E., and Thompson, D.: PRYSM: An open-source framework for PROXY System Modeling, with applications to oxygen-isotope systems, *Journal of Advances in Modeling Earth Systems*, 7, 1220–1247, 2015a.

Dee, S., Noone, D., Buenning, N., Emile-Geay, J., and Zhou, Y.: SPEEDY-IER: A fast atmospheric GCM with water isotope physics, *Journal 920 of Geophysical Research: Atmospheres*, 120, 73–91, 2015b.

Dee, S. G., Steiger, N. J., Emile-Geay, J., and Hakim, G. J.: On the utility of proxy system models for estimating climate states over the Common Era, *Journal of Advances in Modeling Earth Systems*, 8, 1164–1179, 2016.

Deser, C., Phillips, A., Bourdette, V., and Teng, H.: Uncertainty in climate change projections: the role of internal variability, *Climate dynamics*, 38, 527–546, 2012.

925 Dubinkina, S. and Goosse, H.: An assessment of particle filtering methods and nudging for climate state reconstructions, *Climate of the Past*, 9, 1141–1152, 2013.

Esper, J., Frank, D. C., Wilson, R. J., and Briffa, K. R.: Effect of scaling and regression on reconstructed temperature amplitude for the past millennium, *Geophysical Research Letters*, 32, 2005.

Evans, M. N., Kaplan, A., and Cane, M. A.: Optimal sites for coral-based reconstruction of global sea surface temperature, *Paleoceanography*, 930 13, 502–516, 1998.

Evans, M. N., Kaplan, A., Cane, M. A., and Villalba, R.: Globality and Optimality in Climate Field Reconstructions from Proxy Data, in: *Interhemispheric Climate Linkages*, edited by Markgraf, V., pp. 53–72, Cambridge University Press, Cambridge, UK, 2001.

Evans, M. N., Tolwinski-Ward, S. E., Thompson, D. M., and Anchukaitis, K. J.: Applications of proxy system modeling in high resolution paleoclimatology, *Quaternary science reviews*, 76, 16–28, 2013.

935 Evensen, G.: Sequential data assimilation with a nonlinear quasi-geostrophic model using Monte Carlo methods to forecast error statistics, *Journal of Geophysical Research: Oceans*, 99, 10 143–10 162, 1994.

Evensen, G.: The ensemble Kalman filter: Theoretical formulation and practical implementation, *Ocean Dynamics*, 53, 343–367, 2003.

Fang, S.-w., Khodri, M., Timmreck, C., Zanchettin, D., and Jungclaus, J.: Disentangling internal and external contributions to Atlantic multidecadal variability over the past millennium, *Geophysical Research Letters*, 48, e2021GL095 990, 2021.

940 Fernández-Donado, L., González-Rouco, J., Raible, C., Ammann, C., Barriopedro, D., García-Bustamante, E., Jungclaus, J. H., Lorenz, S., Luterbacher, J., Phipps, S. J., et al.: Large-scale temperature response to external forcing in simulations and reconstructions of the last millennium, *Climate of the Past*, 9, 393–421, 2013.

Frank, D., Esper, J., and Cook, E. R.: Adjustment for proxy number and coherence in a large-scale temperature reconstruction, *Geophysical Research Letters*, 34, 2007.

945 Franke, J., Valler, V., Brönnimann, S., Neukom, R., and Jaume-Santero, F.: The importance of input data quality and quantity in climate field reconstructions – results from the assimilation of various tree-ring collections, *Climate of the Past*, 16, 1061–1074, <https://doi.org/10.5194/cp-16-1061-2020>, 2020.

Galmarini, S., Cannon, A. J., Ceglar, A., Christensen, O. B., de Noblet-Ducoudré, N., Dentener, F., Doblas-Reyes, F. J., Dosio, A., Gutierrez, J. M., Iturbide, M., et al.: Adjusting climate model bias for agricultural impact assessment: How to cut the mustard, *Climate services*, 13, 950 65–69, 2019.

Gaspari, G. and Cohn, S. E.: Construction of correlation functions in two and three dimensions, *Quarterly Journal of the Royal Meteorological Society*, 125, 723–757, 1999.

Gebbie, G.: How much did glacial North Atlantic water shoal?, *Paleoceanography*, 29, 190–209, 2014.

Gong, D. and Wang, S.: Definition of Antarctic oscillation index, *Geophysical Research Letters*, 26, 459–462, 1999.

955 Goosse, H., Renssen, H., Timmermann, A., Bradley, R. S., and Mann, M. E.: Using paleoclimate proxy-data to select optimal realisations in an ensemble of simulations of the climate of the past millennium, *Climate Dynamics*, 27, 165–184, 2006.

Goosse, H., Crespin, E., de Montety, A., Mann, M., Renssen, H., and Timmermann, A.: Reconstructing surface temperature changes over the past 600 years using climate model simulations with data assimilation, *Journal of Geophysical Research: Atmospheres*, 115, 2010.

960 Goosse, H., Crespin, E., Dubinkina, S., Loutre, M.-F., Mann, M. E., Renssen, H., Sallaz-Damaz, Y., and Shindell, D.: The role of forcing and internal dynamics in explaining the “Medieval Climate Anomaly”, *Climate dynamics*, 39, 2847–2866, 2012a.

Goosse, H., Guiot, J., Mann, M. E., Dubinkina, S., and Sallaz-Damaz, Y.: The Medieval Climate Anomaly in Europe: Comparison of the summer and annual mean signals in two reconstructions and in simulations with data assimilation, *Global and Planetary Change*, 84, 35–47, 2012b.

965 Gulev, S. K., Thorne, P. W., Ahn, J., Dentener, F. J., Domingues, C. M., Gerland, S., Gong, D., Kaufman, D. S., Nnamchi, H. C., Quaas, J., Rivera, J. A., Sathyendranath, S., Smith, S. L., Trewin, B., von Shuckmann, K., and Vose, R. S.: Changing State of the Climate System, in: *Climate Change 2021: The Physical Science Basis. Contribution of Working Group I to the Sixth Assessment Report of the Intergovernmental Panel on Climate Change*, edited by Masson-Delmotte, V., Zhai, P., Pirani, A., Connors, S. L., Péan, C., Berger, S., Caud, N., Chen, Y., Goldfarb, L., Gomis, M. I., Huang, M., Leitzell, K., Lonnoy, E., Matthews, J. B. R., Maycock, T. K., Waterfield, T., Yelekçi, O., Yu, R., and Zhou, B., chap. 2, Cambridge University Press, 2021.

970 Guttman, N. B.: A sensitivity analysis of the Palmer Hydrologic Drought Index, *JAWRA Journal of the American Water Resources Association*, 27, 797–807, 1991.

Hakim, G. J., Emile-Geay, J., Steig, E. J., Noone, D., Anderson, D. M., Tardif, R., Steiger, N., and Perkins, W. A.: The Last Millennium Climate Reanalysis project: Framework and first results, *Journal of Geophysical Research: Atmospheres*, 121, 6745–6764, 2016.

975 Hamill, T. M., Whitaker, J. S., and Snyder, C.: Distance-dependent filtering of background error covariance estimates in an ensemble Kalman filter, *Monthly Weather Review*, 129, 2776–2790, 2001.

Hansen, J., Sato, M., Russell, G., and Kharecha, P.: Climate sensitivity, sea level and atmospheric carbon dioxide, *Philosophical Transactions of the Royal Society A: Mathematical, Physical and Engineering Sciences*, 371, 20120294, 2013.

Hargreaves, J. and Annan, J.: On the importance of paleoclimate modelling for improving predictions of future climate change, *Climate of the Past*, 5, 803–814, 2009.

980 Hargreaves, J., Abe-Ouchi, A., and Annan, J.: Linking glacial and future climates through an ensemble of GCM simulations, *Climate of the Past*, 3, 77–87, 2007.

Hegerl, G. C., Crowley, T. J., Hyde, W. T., and Frame, D. J.: Climate sensitivity constrained by temperature reconstructions over the past seven centuries, *Nature*, 440, 1029–1032, 2006.

Kalman, R. E.: A new approach to linear filtering and prediction problems, 1960.

985 Kay, J. E., Deser, C., Phillips, A., Mai, A., Hannay, C., Strand, G., Arblaster, J. M., Bates, S., Danabasoglu, G., Edwards, J., et al.: The Community Earth System Model (CESM) large ensemble project: A community resource for studying climate change in the presence of internal climate variability, *Bulletin of the American Meteorological Society*, 96, 1333–1349, 2015.

King, J., Anchukaitis, K. J., Allen, K., Vance, T., and Hessl, A.: Trends and variability in the Southern Annular Mode over the Common Era, *Nature Communications*, 14, 2324, 2023.

990 King, J. M., Anchukaitis, K. J., Tierney, J. E., Hakim, G. J., Emile-Geay, J., Zhu, F., and Wilson, R.: A data assimilation approach to last millennium temperature field reconstruction using a limited high-sensitivity proxy network, *Journal of Climate*, 34, 7091–7111, 2021.

Kurahashi-Nakamura, T., Losch, M., and Paul, A.: Can sparse proxy data constrain the strength of the Atlantic meridional overturning circulation?, *Geoscientific Model Development*, 7, 419–432, 2014.

Kurahashi-Nakamura, T., Paul, A., and Losch, M.: Dynamical reconstruction of the global ocean state during the Last Glacial Maximum, 995 *Paleoceanography*, 32, 326–350, 2017.

Kutzbach, J. E., He, F., Vavrus, S. J., and Ruddiman, W. F.: The dependence of equilibrium climate sensitivity on climate state: Applications to studies of climates colder than present, *Geophysical Research Letters*, 40, 3721–3726, 2013.

LeGrand, P. and Wunsch, C.: Constraints from paleotracer data on the North Atlantic circulation during the last glacial maximum, *Paleoceanography*, 10, 1011–1045, 1995.

1000 Liu, H., Liu, Z., and Lu, F.: A Systematic Comparison of Particle Filter and EnKF in Assimilating Time-Averaged Observations, *Journal of Geophysical Research: Atmospheres*, 122, 13–155, 2017.

Mairesse, A., Goosse, H., Mathiot, P., Wanner, H., and Dubinkina, S.: Investigating the consistency between proxy-based reconstructions and climate models using data assimilation: a mid-Holocene case study, *Climate of the Past*, 9, 2741–2757, 2013.

Malevich, S. B., Vetter, L., and Tierney, J. E.: Global Core Top Calibration of δ 18O in Planktic Foraminifera to Sea Surface Temperature, 1005 *Paleoceanography and Paleoclimatology*, 34, 1292–1315, 2019.

Matsikaris, A., Widmann, M., and Jungclaus, J. H.: On-line and off-line data assimilation in palaeoclimatology: a case study, *Climate of the Past*, 11, 81–93, 2015.

Morales, M. S., Cook, E. R., Barichivich, J., Christie, D. A., Villalba, R., LeQuesne, C., Srur, A. M., Ferrero, M. E., González-Reyes, Á., Couvreux, F., et al.: Six hundred years of South American tree rings reveal an increase in severe hydroclimatic events since mid-20th century, *Proceedings of the National Academy of Sciences*, 117, 16 816–16 823, 2020.

1010 Neukom, R., Barboza, L. A., Erb, M. P., Shi, F., Emile-Geay, J., Evans, M. N., Franke, J., Kaufman, D. S., Lücke, L., Rehfeld, K., et al.: Consistent multi-decadal variability in global temperature reconstructions and simulations over the Common Era, *Nature geoscience*, 12, 643, 2019.

Oke, P. R., Allen, J. S., Miller, R. N., Egbert, G. D., and Kosro, P. M.: Assimilation of surface velocity data into a primitive equation coastal ocean model, *Journal of Geophysical Research: Oceans*, 107, 5–1, 2002.

Osman, M. B., Tierney, J. E., Zhu, J., Tardif, R., Hakim, G. J., King, J., and Poulsen, C. J.: Globally resolved surface temperatures since the Last Glacial Maximum, *Nature*, 599, 239–244, 2021.

Otto-Bliesner, B. L., Brady, E. C., Fasullo, J., Jahn, A., Landrum, L., Stevenson, S., Rosenbloom, N., Mai, A., and Strand, G.: Climate variability and change since 850 CE: An ensemble approach with the Community Earth System Model, *Bulletin of the American Meteorological Society*, 97, 735–754, 2016.

Overpeck, J. T., Otto-Bliesner, B. L., Miller, G. H., Muhs, D. R., Alley, R. B., and Kiehl, J. T.: Paleoclimatic evidence for future ice-sheet instability and rapid sea-level rise, *Science*, 311, 1747–1750, 2006.

Parsons, L. A., Amrhein, D. E., Sanchez, S. C., Tardif, R., Brennan, M. K., and Hakim, G. J.: Do Multi-Model Ensembles Improve Reconstruction Skill in Paleoclimate Data Assimilation?, *Earth and Space Science*, 8, e2020EA001467, 2021.

1025 Perkins, W. A. and Hakim, G.: Linear inverse modeling for coupled atmosphere-ocean ensemble climate prediction, *Journal of Advances in Modeling Earth Systems*, 12, e2019MS001778, 2020.

Perkins, W. A. and Hakim, G. J.: Reconstructing paleoclimate fields using online data assimilation with a linear inverse model, *Climate of the Past*, 13, 421–436, 2017.

Rice, J. L., Woodhouse, C. A., and Lukas, J. J.: Science and Decision Making: Water Management and Tree-Ring Data in the Western United States, *JAWRA Journal of the American Water Resources Association*, 45, 1248–1259, 2009.

1030 Rohling, E., Sluijs, A., Dijkstra, H., Köhler, P., van de Wal, R., von der Heydt, A., Beerling, D., Berger, A., Bijl, P., Crucifix, M., et al.: Making sense of palaeoclimate sensitivity, *Nature*, 491, 683–691, 2012.

Rohling, E. J., Marino, G., Foster, G. L., Goodwin, P. A., Von der Heydt, A. S., and Köhler, P.: Comparing climate sensitivity, past and present, *Annual Review of Marine Science*, 10, 261–288, 2018.

1035 Schmidt, G., Annan, J., Bartlein, P., Cook, B., Guiyadi, E., Hargreaves, J., Harrison, S., Kageyama, M., LeGrande, A., Konecky, B., et al.: Using paleo-climate comparisons to constrain future projections in CMIP5., *Climate of the Past Discussions*, 9, 2013.

Schmidt, G. A.: Enhancing the relevance of palaeoclimate model/data comparisons for assessments of future climate change, *Journal of Quaternary Science*, 25, 79–87, 2010.

Sherwood, S., Webb, M. J., Annan, J. D., Armour, K. C., Forster, P. M., Hargreaves, J. C., Hegerl, G., Klein, S. A., Marvel, K. D., Rohling, 1040 E. J., et al.: An assessment of Earth's climate sensitivity using multiple lines of evidence, *Reviews of Geophysics*, 58, e2019RG000678, 2020.

Smerdon, J. E.: Climate models as a test bed for climate reconstruction methods: pseudoproxy experiments, *Wiley Interdisciplinary Reviews: Climate Change*, 3, 63–77, 2012.

Snyder, C. W.: The value of paleoclimate research in our changing climate, *Climatic Change*, 100, 407–418, 2010.

1045 Steiger, N. J., Hakim, G. J., Steig, E. J., Battisti, D. S., and Roe, G. H.: Assimilation of time-averaged pseudoproxies for climate reconstruction, *Journal of Climate*, 27, 426–441, 2014.

Steiger, N. J., Steig, E. J., Dee, S. G., Roe, G. H., and Hakim, G. J.: Climate reconstruction using data assimilation of water isotope ratios from ice cores, *Journal of Geophysical Research: Atmospheres*, 122, 1545–1568, 2017.

Steiger, N. J., Smerdon, J. E., Cook, E. R., and Cook, B. L.: A reconstruction of global hydroclimate and dynamical variables over the 1050 Common Era, *Scientific Data*, 5, <https://doi.org/10.1086/sdata.2018.86>, 2018.

Stevenson, S., Otto-Bliesner, B., Brady, E., Nusbaumer, J., Tabor, C., Tomas, R., Noone, D., and Liu, Z.: Volcanic eruption signatures in the isotope-enabled last millennium ensemble, *Paleoceanography and Paleoclimatology*, 34, 1534–1552, 2019.

Tardif, R., Hakim, G. J., Perkins, W. A., Horlick, K. A., Erb, M. P., Emile-Geay, J., Anderson, D. M., Steig, E. J., and Noone, D.: Last Millennium Reanalysis with an expanded proxy database and seasonal proxy modeling., *Climate of the Past*, 15, 1251–1273, 2019.

1055 Tierney, J. E. and Tingley, M. P.: A Bayesian, spatially-varying calibration model for the TEX86 proxy, *Geochimica et Cosmochimica Acta*, 127, 83–106, 2014.

Tierney, J. E. and Tingley, M. P.: BAYSPLINE: A new calibration for the alkenone paleothermometer, *Paleoceanography and Paleoclimatology*, 33, 281–301, 2018.

Tierney, J. E., Malevich, S. B., Gray, W., Vetter, L., and Thirumalai, K.: Bayesian calibration of the Mg/Ca paleothermometer in planktic foraminifera, *Paleoceanography and Paleoclimatology*, 34, 2005–2030, 2019.

1060 Tierney, J. E., Poulsen, C. J., Montañez, I. P., Bhattacharya, T., Feng, R., Ford, H. L., Hönisch, B., Inglis, G. N., Petersen, S. V., Sagoo, N., et al.: Past climates inform our future, *Science*, 370, eaay3701, 2020a.

Tierney, J. E., Zhu, J., King, J., Malevich, S. B., Hakim, G. J., and Poulsen, C. J.: Glacial cooling and climate sensitivity revisited, *Nature*, 584, 569–573, 2020b.

1065 Tierney, J. E., Zhu, J., Li, M., Ridgwell, A., Hakim, G. J., Poulsen, C. J., Whiteford, R. D., Rae, J. W., and Kump, L. R.: Spatial patterns of climate change across the Paleocene–Eocene Thermal Maximum, *Proceedings of the National Academy of Sciences*, 119, e2205326 119, 2022.

Tolwinski-Ward, S. E., Evans, M. N., Hughes, M. K., and Anchukaitis, K. J.: An efficient forward model of the climate controls on interannual variation in tree-ring width, *Climate Dynamics*, 36, 2419–2439, 2011.

1070 Valler, V., Franke, J., and Brönnimann, S.: Impact of different estimations of the background-error covariance matrix on climate reconstructions based on data assimilation, *Climate of the Past*, 15, 1427–1441, 2019.

Van der Schrier, G., Jones, P., and Briffa, K.: The sensitivity of the PDSI to the Thornthwaite and Penman-Monteith parameterizations for potential evapotranspiration, *Journal of Geophysical Research: Atmospheres*, 116, 2011.

Van Leeuwen, P. J.: Particle filtering in geophysical systems, *Monthly Weather Review*, 137, 4089–4114, 2009.

1075 Vrac, M.: Multivariate bias adjustment of high-dimensional climate simulations: the Rank Resampling for Distributions and Dependences (R 2 D 2) bias correction, *Hydrology and Earth System Sciences*, 22, 3175–3196, 2018.

Wang, Q. and Robertson, D.: Multisite probabilistic forecasting of seasonal flows for streams with zero value occurrences, *Water Resources Research*, 47, 2011.

Wang, Q., Shrestha, D. L., Robertson, D., and Pokhrel, P.: A log-sinh transformation for data normalization and variance stabilization, *Water Resources Research*, 48, 2012.

1080 Whitaker, J. S. and Hamill, T. M.: Ensemble data assimilation without perturbed observations, *Monthly Weather Review*, 130, 1913–1924, 2002.

Wikle, C. K. and Berliner, L. M.: A Bayesian tutorial for data assimilation, *Physica D: Nonlinear Phenomena*, 230, 1–16, 2007.

Wilson, R., Anchukaitis, K., Briffa, K. R., Büntgen, U., Cook, E., D'arrigo, R., Davi, N., Esper, J., Frank, D., Gunnarson, B., et al.: Last 1085 millennium northern hemisphere summer temperatures from tree rings: Part I: The long term context, *Quaternary Science Reviews*, 134, 1–18, 2016.

Winguth, A., Archer, D., Maier-Reimer, E., and Mikolajewicz, U.: Paleonutrient data analysis of the glacial Atlantic using an adjoint ocean general circulation model, in: *Inverse Methods in Global Biogeochemical Cycles*, pp. 171–183, Wiley Online Library, 2000.

Zhao, T., Bennett, J. C., Wang, Q., Schepen, A., Wood, A. W., Robertson, D. E., and Ramos, M.-H.: How suitable is quantile mapping for 1090 postprocessing GCM precipitation forecasts?, *Journal of Climate*, 30, 3185–3196, 2017.

Zhu, F., Emile-Geay, J., Hakim, G. J., King, J., and Anchukaitis, K. J.: Resolving the differences in the simulated and reconstructed temperature response to volcanism, *Geophysical Research Letters*, 47, e2019GL086 908, 2020a.

Zhu, F., Emile-Geay, J., Anchukaitis, K. J., Hakim, G. J., Wittenberg, A. T., Morales, M. S., Toohey, M., and King, J.: A re-appraisal of the ENSO response to volcanism with paleoclimate data assimilation, *Nature communications*, 13, 1–9, 2022.

1095 Zhu, J., Liu, Z., Brady, E., Otto-Bliesner, B., Zhang, J., Noone, D., Tomas, R., Nusbaumer, J., Wong, T., Jahn, A., et al.: Reduced ENSO variability at the LGM revealed by an isotope-enabled Earth system model, *Geophysical Research Letters*, 44, 6984–6992, 2017.

Zhu, J., Poulsen, C. J., and Otto-Bliesner, B. L.: High climate sensitivity in CMIP6 model not supported by paleoclimate, *Nature Climate Change*, 10, 378–379, 2020b.

1100 Zhu, J., Otto-Bliesner, B. L., Brady, E. C., Gettelman, A., Bacmeister, J. T., Neale, R. B., Poulsen, C. J., Shaw, J. K., McGraw, Z. S., and Kay, J. E.: LGM paleoclimate constraints inform cloud parameterizations and equilibrium climate sensitivity in CESM2, *Journal of Advances in Modeling Earth Systems*, p. e2021MS002776, 2021a.

Zhu, J., Otto-Bliesner, B. L., Brady, E. C., Poulsen, C. J., Tierney, J. E., Lofverstrom, M., and DiNezio, P.: Assessment of equilibrium climate sensitivity of the Community Earth System Model version 2 through simulation of the Last Glacial Maximum, *Geophysical Research Letters*, 48, e2020GL091 220, 2021b.

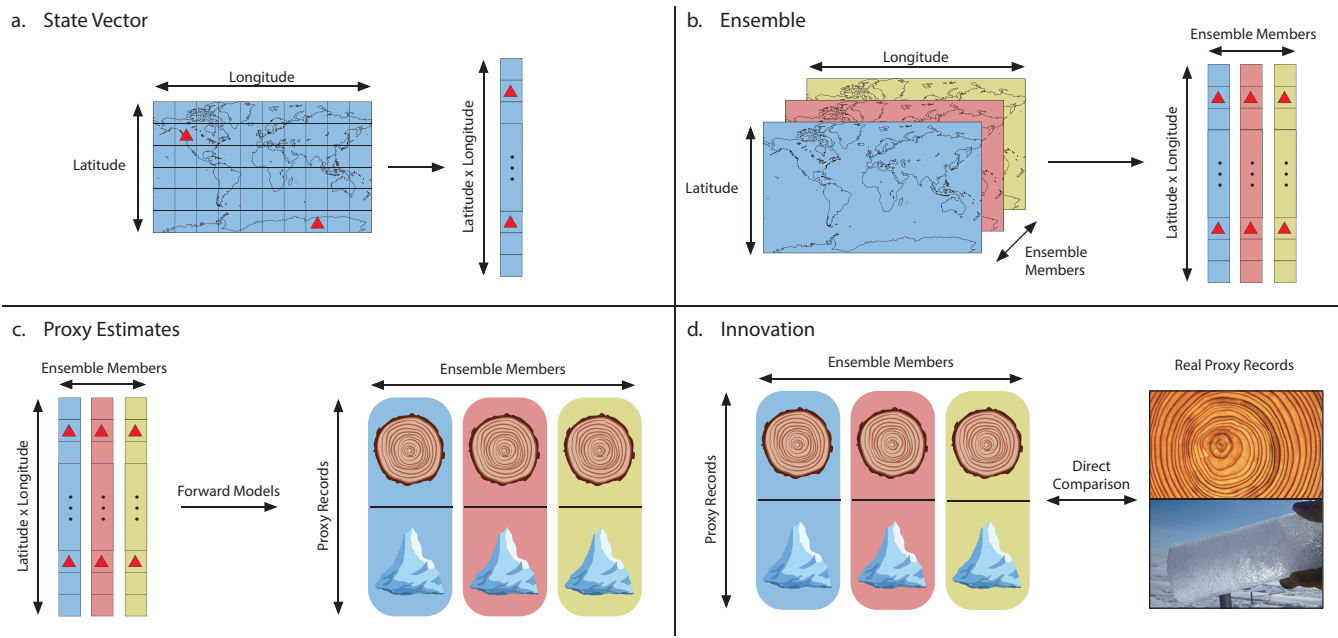


Figure 1. Illustration of common tasks and vocabulary for paleoclimate data assimilation. **Top-left:** (a) Gridded climate model output is reshaped into a *state vector*. Red triangles indicate the location of proxy records. **Top-right:** (b) Multiple climate model outputs are reshaped into state vectors and concatenated into an *ensemble*. **Bottom-left:** (c) Forward models are applied to each state vector and used to generate *proxy estimates* for each proxy record. **Bottom-right:** (d) Proxy estimates are compared directly to the real proxy records. The difference between the estimates and the real records is the *innovation*.

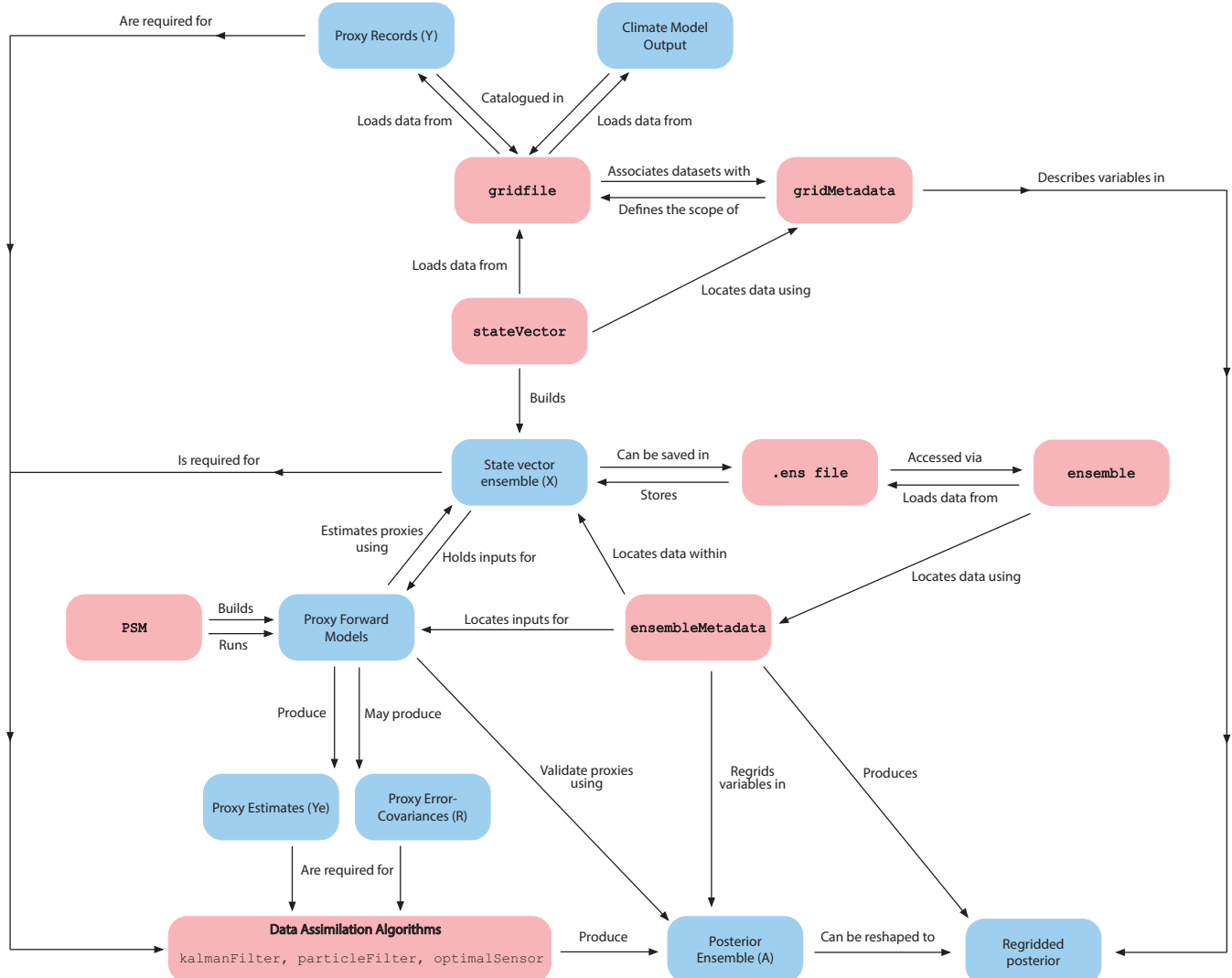


Figure 2. Flowchart illustrating DASH components and their uses within the context of paleoclimate data assimilation workflows.

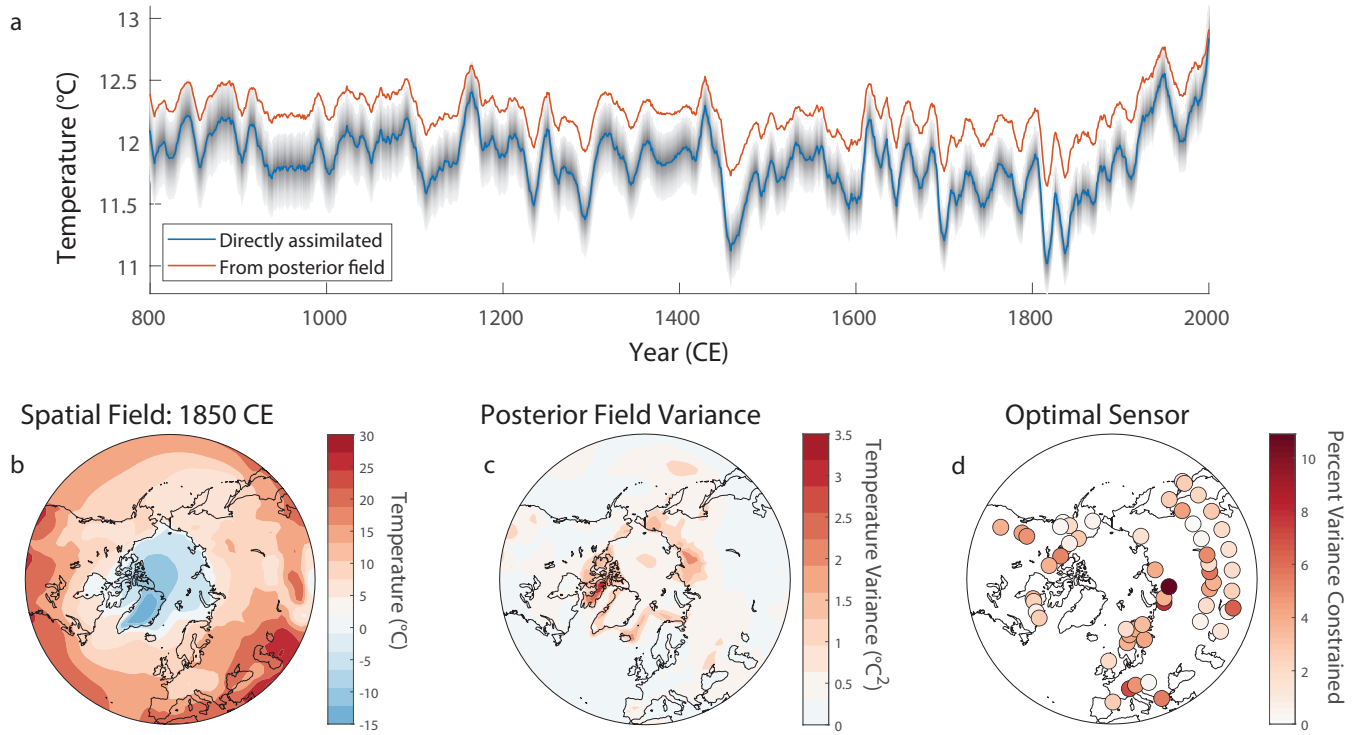


Figure 3. Results from Example 1, the NTREND assimilation. **Top:** (a) Reconstructed mean extratropical summer (June-August) temperatures. The blue line shows the reconstructed index when the index is assimilated directly in the state vector. The red line shows the index calculated from the posterior spatial field. Grey shading indicates the 5-95% confidence level for Index 1. **Lower-left:** (b) The reconstructed summer-temperature spatial field in the year 1850 CE. **Lower-center:** (c) The variance of the posterior spatial field in the year 1850 CE. High variance indicates greater uncertainty in the reconstructed spatial field. **Lower-right:** (d) Results of the optimal sensor analysis. Circles indicate the locations of the NTREND tree-ring records. The color of each circle indicates the percent variance of the reconstructed index that is constrained by assimilating each NTREND site individually.

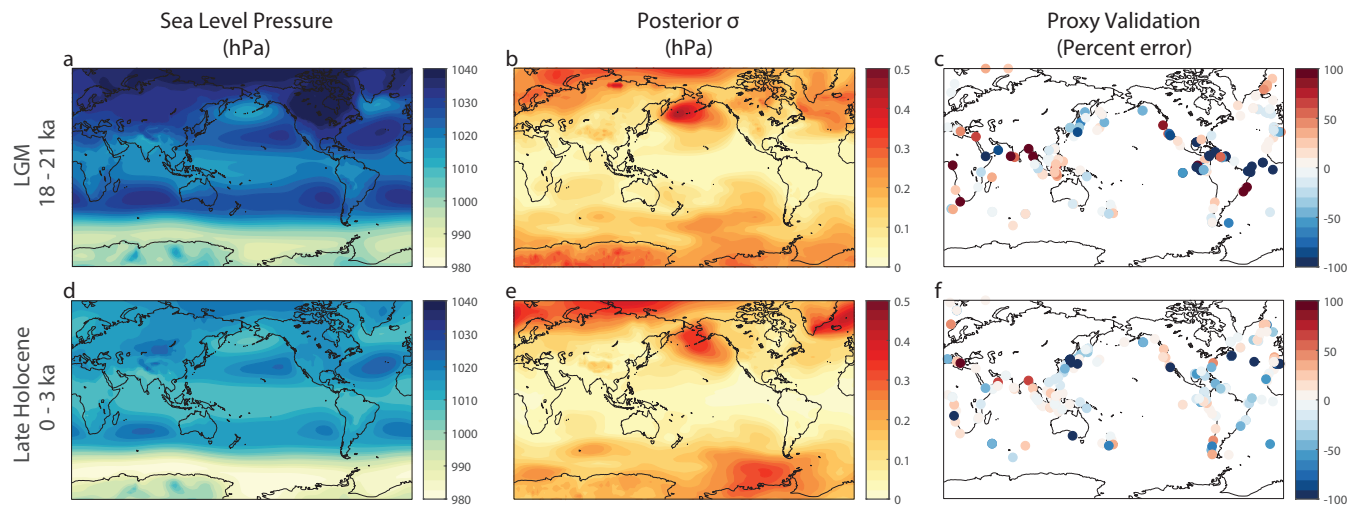


Figure 4. Results from Example 2, the LGM assimilation. **Upper row shows results (a,b,c) Results** for the Last Glacial Maximum (18-21 ka); **lower row shows results (d,e,f) Results** for the late Holocene (0-3 ka). **From left to right (a,c) display reconstructed (d,e) Reconstructed** sea level pressure fields (in hPa), (b,f) the standard deviation across the posterior ensembles for each reconstructed field (in hPa), (c,f) and the absolute (f) Absolute percent errors from the proxy validation.

Table 1. Proxy forward-models currently supported by DASH.

Model	Description	Citation or Authors	Github Repository
BayFOX	Bayesian model of planktic foraminiferal $\delta^{18}O_c$	Malevich et al. (2019)	jesstierney/bayfoxm
BayMAG	Bayesian model of planktic foraminiferal Mg/Ca	Tierney et al. (2019)	jesstierney/BAYMAG
BaySPAR	Bayesian model for TEX'86	Tierney and Tingley (2014)	jesstierney/BAYSPAR
BaySPLINE	Bayesian model for UK'37	Tierney and Tingley (2018)	jesstierney/BAYSPLINE
Identity	The identity function		DASH built-in
Multi-variate Linear	General multi-variate linear forward models		DASH built-in
PDSI	Palmer Drought-Severity Index estimator	Dave Meko, Jonathan King	JonKing93/pdsi
PRYSM Cellulose	Cellulose $\delta^{18}O$	Dee et al. (2015a)	sylvia-dee/PRYSM
PRYSM Coral	Coral $\delta^{18}O$	Dee et al. (2015a)	sylvia-dee/PRYSM
PRYSM Ice-Core	Ice-core $\delta^{18}O$	Dee et al. (2015a)	sylvia-dee/PRYSM
VS-Lite	Vaganov-Shashkin Lite model of tree-ring width	Tolwinski-Ward et al. (2011)	suztolwinskiward/vslite

Example 1: Northern Hemisphere Summer Temperatures over the Last Millennium

```
1  %% Example 1: NTREND Assimilation
2
3  % Reset the random number generator so all examples are reproducible
4  rng('default');
5
6  %% gridfile: Organize climate model output
7
8  % List of climate model output files
9  outputFile1 = 'b.e11.BLMTRC5CN.f19_g16.002.cam.h0.TREFHT.085001-184912.nc';
10 outputFile2 = 'b.e11.BLMTRC5CN.f19_g16.002.cam.h0.TREFHT.185001-200512.nc';
11
12 % Define metadata that spans the climate model output dataset
13 lat = ncread(outputFile1, 'lat');
14 lon = ncread(outputFile1, 'lon');
15 time = datetime(850,1,15):calmonths(1):datetime(2005,12,15);
16
17 metadata = gridMetadata('lat', lat, 'lon', lon, 'time', time);
18 metadata = metadata.addAttribute('Units', 'Kelvin', 'Model', 'CESM 1.0');
19
20 % Initialize a new, empty gridfile to catalogue the dataset
21 modelOutput = gridfile.new('Temperature-CESM', metadata, 'overwrite');
22
23 % Catalogue the source files for the dataset in the gridfile
24 dimensionOrder = ["lon", "lat", "time"];
25 output1Metadata = metadata.index('time', 1:12000);
26 output2Metadata = metadata.index('time', 12001:13872);
27
28 modelOutput.add('netcdf', outputFile1, "TREFHT", dimensionOrder, output1Metadata);
29 modelOutput.add('netcdf', outputFile2, "TREFHT", dimensionOrder, output2Metadata);
30
31 % Convert loaded data from Kelvin to Celsius
32 modelOutput.transform('plus', -273.15);
33
34
35 %% gridfile: Organize climate proxy records
36
37 % File holding the proxy record dataset
38 proxyFile = 'ntrend.mat';
39
40 % Define metadata for the proxy record dataset
41 info = load(proxyFile, 'years', 'site_IDs', 'lons', 'lats', 'seasons');
42 site = [info.site_IDs, info.lats, info.lons, info.seasons];
```

```

43 proxyMetadata = gridMetadata('site', site, 'time', info.years);
44
45 % Catalogue the proxy record dataset in a gridfile
46 proxies = gridfile.new('ntrend', proxyMetadata, 'overwrite');
47 proxies.add('mat', proxyFile, 'crn', ["time" "site"], proxyMetadata);
48
49 % Indicate that -999 is a fill value and should be converted to NaN
50 proxies.fillValue(-999);
51
52
53 %% State vector: Design and build a state vector ensemble
54
55 % Initialize a state vector and label the object
56 sv = stateVector('NTREND Assimilation');
57
58 % Initialize variables that are:
59 % 1. Used to run the proxy forward models, or
60 % 2. Reconstruction targets.
61 proxyNames = proxyMetadata.site(:,1);
62 sv = sv.add(proxyNames, modelOutput);
63 sv = sv.add(["T", "T_index"], modelOutput);
64
65 % Specify that ensemble members will be selected from each year of model output
66 % (Note that we are only using January as a reference month for each year.
67 % Later steps will specify the monthly means used in the assimilation).
68 january = month(metadata.time) == 1;
69 sv = sv.design(-1, 'time', 'ensemble', january);
70
71 % Design the reconstruction targets to use data north of 35N and a seasonal
72 % mean over June, July, and August. Also use a latitude-weighted spatial
73 % mean for the reconstructed extratropical temperature index.
74 extratropical = metadata.lat > 35;
75 JJA = [5 6 7];
76 latWeights = cosd(metadata.lat(extratropical));
77
78 sv = sv.design(["T", "T_index"], 'lat', [], extratropical);
79 sv = sv.mean( ["T", "T_index"], 'time', JJA);
80 sv = sv.weightedMean("T_index", ["lat" "lon"], {latWeights, []});
81
82 % Design the proxy variables to use the site-specific seasonal temperature
83 % mean from the model grid closest to the proxy site.
84 nProxies = numel(proxyNames);
85 proxyCoordinates = str2double( proxyMetadata.site(:,2:3) );
86 [~, latIndices, lonIndices] = dash.closest.latlon(proxyCoordinates, metadata.lat, metadata.lon);

```

```

87 for p = 1:nProxies
88     sv = sv.design(p, ["lat","lon"], [], {latIndices(p), lonIndices(p)} );
89
90     season = strsplit(proxyMetadata.site(p,4), ',');
91     season = str2double(season) - 1;
92     sv = sv.mean(p, 'time', season);
93 end
94
95 % Build a state vector ensemble with 1156 members and save it to file
96 [ens, ensMeta] = sv.build(1156, 'sequential', true, 'file', 'ntrend-ensemble', 'overwrite', true);
97
98
99 %% PSM: Implement forward models for the NTREND sites and estimate proxy values
100
101 % Load coefficients of linear forward models
102 coeffs = load('ntrend-forward-model-coefficients');
103 slopes = coeffs.slopes;
104 intercepts = coeffs.intercepts;
105
106 % Design a univariate linear forward models for each proxy record
107 forwardModels = cell(nProxies, 1);
108 for p = 1:nProxies
109     forwardModels{p} = PSM.linear(slopes(p), intercepts(p));
110
111     % Indicate the row in the state vector ensemble that holds the seasonal
112     % temperature means needed to run the forward model.
113     row = ensMeta.find( proxyNames(p) );
114     forwardModels{p} = forwardModels{p}.rows(row);
115 end
116
117 % Compute proxy estimates by running the forward models on the ensemble
118 Ye = PSM.estimate(forwardModels, ens);
119
120
121 %% Kalman Filter: Implement a Kalman Filter and generate a reconstruction
122
123 % Initialize a Kalman Filter
124 kf = kalmanFilter('NTREND Assimilation');
125
126 % Select the prior. This will be the variables in the ensemble that
127 % correspond to reconstruction targets.
128 ens = ens.useVariables(["T","T_index"]);
129 ensMeta = ens.metadata;
130 kf = kf.prior(ens);

```

```

131
132 % Specify the proxy records and estimates used in assimilation
133 Y = proxies.load;
134 kf = kf.observations(Y);
135 kf = kf.estimates(Ye);
136
137 % Also specify proxy error variances
138 R = load('ntrend-error-variances').R;
139 kf = kf.uncertainties(R);
140
141 % Implement covariance localization with a radius of 20000 km
142 coordinates = ensMeta.latlon;
143 radius = 20000; % km
144 [wloc, yloc] = dash.localize.gc2d(coordinates, proxyCoordinates, radius);
145 kf = kf.localize(wloc, yloc);
146
147 % Also calculate a latitude-weighted, spatial mean temperature index from
148 % the updated spatial field. This will return the full posterior ensemble
149 % for the index, without needing to save the (very large) posterior
150 % ensemble of the full spatial temperature field.
151 rows = ensMeta.find('T');
152 latWeights = cosd(coordinates(rows,1));
153 kf = kf.index('T_index2', 'mean', 'rows', rows, 'weights', latWeights);
154
155 % Save posterior percentiles and variance, rather than the full posterior.
156 kf = kf.percentiles(5:95);
157 kf = kf.variance(true);
158
159 % Run the Kalman Filter.
160 output = kf.run;
161
162 % Extract the updated spatial field and its variance. Regrid to match the
163 % dimensions of the initial climate model output
164 [T, Tmeta] = ensMeta.regrid("T", output.Amean, 'order', ["lat","lon"]);
165 Tvar = ensMeta.regrid("T", output.Avar, 'order', ["lat","lon"]);
166
167 % Also extract the spatial-mean time series and percentiles
168 index1 = output.Amean(end,:);
169 index1p = output.Aperc(end,:,:);
170 index2 = output.index_T_index2;
171
172 % Save for post-processing and visualization
173 time = info.years;
174 save('ntrend-reconstruction.mat','T','Tvar','Tmeta','index1','index1p','index2','time');

```

```
175
176
177 %% Optimal sensor
178
179 % Initialize an optimal sensor for the NTREND assimilation
180 os = optimalSensor('NTREND sensors');
181
182 % Use the summer-temperature spatial mean index as the sensor metric.
183 T = ens.useVariables('T_index').load;
184 os = os.metric(T);
185
186 % Also provide the proxy estimates and error variances for the analysis
187 os = os.estimate(Ye);
188 os = os.uncertainties(R);
189
190 % Run the sensor to evaluate the ability of each record to reduce uncertainty
191 proxyPower = os.evaluate;
192
193 % Save for analysis and visualization
194 save('ntrend-optimal-sensor', 'proxyPower', 'proxyMetadata');
```

Example 2: Global Sea Level Pressures from the Last Glacial Maximum to Present

```
1 %% Example 2: LGM Assimilation
2
3 % Reset the random number generator so all examples are reproducible
4 rng('default');
5
6 %% gridfile: Organize climate model output
7
8 % Climate model output
9 slpFile = 'PSL_cam_50yrDecMon_iCESM_LGMtoPresent.nc';
10 sstFile = 'TEMP_pop_50yrDecMon_iCESM_LGMtoPresent.nc';
11 d18OFile = 'R18O_pop_50yrDecMon_iCESM_LGMtoPresent.nc';
12
13 % Define metadata for the rectilinear, atmospheric model (CAM) output
14 lat = ncread(slpFile, 'lat');
15 lon = ncread(slpFile, 'lon');
16 time = ncread(slpFile, 'time');
17 run = ncread(slpFile, 'run');
18 camMetadata = gridMetadata('lat', lat, 'lon', lon, 'time', time, 'run', run);
19
20 % Define metadata for the tripolar, ocean model (POP) output
21 lat = ncread(sstFile, 'TLAT');
22 lon = ncread(sstFile, 'TLONG');
23 site = [lat(:), lon(:)];
24 popMetadata = gridMetadata('site', site, 'time', time, 'run', run);
25
26 % Initialize a gridfile object for each variable
27 slp = gridfile.new('SLP', camMetadata, 'overwrite');
28 sst = gridfile.new('SST', popMetadata, 'overwrite');
29 d18O = gridfile.new('d18O', popMetadata, 'overwrite');
30
31 % Catalogue the output files
32 slp.add('netcdf', slpFile, "PSL", [ "lon", "lat", "time", "run"], camMetadata);
33 sst.add('netcdf', sstFile, "TEMP", [ "site", "site", "time", "run"], popMetadata);
34 d18O.add('netcdf', d18OFile, "R18O", [ "site", "site", "time", "run"], popMetadata);
35
36
37 %% gridfile: Organize climate proxy records
38
39 % File holding the proxy record dataset and metadata
40 proxyFile = 'proxies.mat';
41
42 % Define metadata for the proxy record dataset
```

```

43 info = load(proxyFile, 'ID', 'lat', 'lon', 'species', 'type', 'time', 'timeUnits');
44 site = [info.ID, info.lat, info.lon, info.type, info.species];
45 proxyMetadata = gridMetadata('site', site, 'time', info.time);
46
47 % Catalogue the proxy record dataset in a gridfile
48 proxies = gridfile.new('proxies', proxyMetadata, 'overwrite');
49 proxies.add('mat', proxyFile, "Y", ["time","site"], proxyMetadata);
50
51
52 %% Design and build state vector ensemble
53
54 % Initialize and label a stateVector object
55 sv = stateVector('LGM Assimilation');
56
57 % Initialize variables
58 % Reconstruction target: Sea level pressure (SLP)
59 % Forward models inputs: Sea surface temperature (SST), d18O of sea water
60 sv = sv.add(["SLP","SST","d18O"], [slp;sst;d18O]);
61
62 % Specify that ensemble members should be selected from the different runs
63 % and time slices. Use January of each time slice as a reference point
64 january = camMetadata.time(:,1)==1;
65 sv = sv.design(-1, ["time","run"], 'ensemble', {january,[]});
66
67 % Use annual mean values for all variables
68 months = (0:11)'; % Indices of months relative to the January reference point
69 sv = sv.mean(-1, 'time', months);
70
71 % Build the state vector sequentially using all available 50-year bins.
72 % Save to the file "lgm-ensemble.ens"
73 [ens, ensMeta] = sv.build('all', 'sequential', true, 'file', 'lgm-ensemble', 'overwrite', true);
74
75 % There are 16 50-year bins for each of the nine 3,000 year intervals.
76 % Use the sets of 16 ensemble members to build an evolving ensemble for the
77 % nine intervals.
78 members = 1:ens.nMembers;
79 members = reshape(members, 9, 16)';
80 ens = ens.evolving(members);
81
82
83 %% PSM: Implement forward models for the proxy sites and estimate proxy values
84
85 % Download proxy forward models from Github
86 PSM.download('bayfox');

```

```

87 PSM.download('bayspline');
88
89 % Design a forward model for each proxy record
90 nProxies = numel(info.ID);
91 forwardModels = cell(nProxies, 1);
92 for p = 1:nProxies
93
94     % Get the proxy ID, location, and type
95     ID          = proxyMetadata.site(p, 1);
96     coordinates = proxyMetadata.site(p, 2:3);
97     coordinates = str2double(coordinates);
98     type         = proxyMetadata.site(p, 4);
99
100    % Use either a UK'37 forward model, which requires SSTs as input
101    if type == "uk37"
102        model = PSM.bayspline;
103        SST   = ensMeta.closestLatLon("SST", coordinates, 'site', [1 2]);
104        model = model.rows(SST);
105
106    % Or a d180_c model, which is calibrated to different foraminiferal species...
107    elseif type == "d180c"
108        species = proxyMetadata.site(p,5);
109        model   = PSM.bayfox(species);
110
111        % ...and which requires SSTs and d180_sw as input
112        SST   = ensMeta.closestLatLon( "SST", coordinates, 'site', [1 2]);
113        d180  = ensMeta.closestLatLon("d180", coordinates, 'site', [1 2]);
114        model = model.rows([SST;d180]);
115    end
116
117    % Label and save the model for each proxy
118    model = model.label(ID);
119    forwardModels{p} = model;
120 end
121
122 % Run the forward models on the inputs from the ensemble to compute proxy
123 % estimates and proxy error variances
124 [Ye, R] = PSM.estimate(forwardModels, ens.load);
125 R = squeeze(mean(R,2));
126
127 %% Kalman Filter
128
129 % Initialize and label a kalman filter
130 kf = kalmanFilter('LGM Assimilation');

```

```

131
132 % Provide the proxy records, prior, estimates, and error variances to the filter
133 Y = proxies.load;
134 kf = kf.prior(ens);
135 kf = kf.observations(Y);
136 kf = kf.estimates(Ye);
137 kf = kf.uncertainties(R);
138
139 % Run the Kalman filter. To conserve memory, return the mean and variance
140 % of the posterior ensemble, rather than the complete ensemble
141 kf = kf.variance(true);
142 output = kf.run;
143
144 % Regrid the SLP reconstruction target
145 [SLP, SLPmeta] = ensMeta.regrid("SLP", output.Amean, 'order', ["lat","lon"]);
146 SLPvar = ensMeta.regrid("SLP", output.Avar, 'order', ["lat","lon"]);
147
148 % Save for visualization
149 save('lgm-reconstruction', 'SLP', 'SLPmeta', 'SLPvar');
150
151
152 %% Proxy validation: Run the proxy system models on the posterior ensemble
153
154 % Run the proxy forward models using inputs from the posterior ensemble
155 Ypost = PSM.estimate(forwardModels, output.Amean);
156
157 % Save for post-processing and visualization
158 save('lgm-proxy-validation', 'Ypost', 'proxyMetadata');

```